DEVELOPMENT OF A CARBON FIBER REINFORCED POLYMER PRESTRESSING SYSTEM FOR STRUCTURAL APPLICATIONS

by

Clayton A. Burningham

A dissertation submitted to the faculty of
The University of Utah
in partial fulfillment of the requirements for the degree of

Doctor of Philosophy

Department of Civil and Environmental Engineering

The University of Utah

December 2011

The University of Utah Graduate School

STATEMENT OF DISSERTATION APPROVAL

The dissertation of **Clayton A. Burningham**

has been approved by the following supervisory committee members:

Chris P. Pantelides	, Chair	**10/26/11** Date Approved
Lawrence D. Reaveley	, Member	**10/26/11** Date Approved
Paul J. Tikalsky	, Member	**10/26/11** Date Approved
Charles B. Elliott	, Member	**10/26/11** Date Approved
Daniel O. Adams	, Member	**10/26/11** Date Approved

and by **Paul J. Tikalsky** , Chair of

the Department of **Civil and Environmental Engineering**

and by Charles A. Wight, Dean of The Graduate School.

ABSTRACT

Prestressed concrete has been a significant contributor to the success of modern civil engineering projects because it allows longer spans and lighter members to be constructed. Despite the usefulness of prestressed concrete, a major disadvantage is the susceptibility of steel prestressing tendons to corrosion. Corrosion can be accelerated by vehicular impact damage which removes concrete cover, exposing the tendons to the elements. If damaged members can be repaired with fiber reinforced polymer (FRP) composites, total replacement of the structure can be avoided. FRP composites are excellent candidates for use in prestressing because of their light weight, superior resistance to corrosion, and comparable strength to steel.

Post-tensioned external FRP tendons can be implemented to restore capacity lost through corrosion or damage or meet increased load requirements; however, there are three obstacles that have hindered wide implementation of external FRP post-tensioning in rehabilitation and retrofit applications. The following obstacles inhibit implementation: the lack of a suitable anchorage device to maintain the post-tensioning force in the FRP tendons, the lack of an innovative stressing device that reduces the requirement for a significant amount of free space behind the post-tensioned member, and the lack of design equations detailing the use of FRP tendons for field applications.

This research involves overcoming the three aforementioned obstacles. The first part of this research is concerned with the development of a unibody clamp anchor that

controls slip and stress concentrations in post-tensioned carbon fiber reinforced polymer (CFRP) rods. Additionally, finite element modeling was employed to conduct a relative comparison of the anchor performance across four different design generations. A second objective of the research was to design and implement a simple mechanical stressing device and the unibody clamp anchors to damaged reinforced concrete beams controlled by shear and damaged prestressed concrete beams controlled by flexure. The final objective considered in the research was an evaluation of design equations from the literature. In short, this research as a whole demonstrates the ability to utilize external post-tensioned CFRP rods for structural repair applications, and forecasts their potential for more widespread use.

TABLE OF CONTENTS

ACKNOWLEDGEMENTS

I would like to thank my mentors and friends Dr. Chris Pantelides and Dr. Larry Reaveley for their support and guidance during my educational pursuits. Additionally, I wish to thank committee members Dr. Paul Tikalsky, Dr. Torch Elliott, and Dr. Dan Adams for their support and dedication.

I am grateful to Utah Department of Transportation, Geneva Rock Products, Inc., Hanson Structural Precast, and Sika Inc. Without their contributions this research would not have been possible. Further thanks goes to Brandon Besser, Megan Crump, Jack Furbush, Mike Gibbons, Ruifen Liu, Yasuteru Okahashi, Brett Raddon, Uma Ramasamy, Tyler Ross, Eric Smith, Max Wood, and Arthur Yeomans for their assistance in specimen fabrication, laboratory testing, and computer modeling.

Thank you to Mark Bryant for his unwavering dedication to all of the students in the Civil and Environmental Engineering Department at the University of Utah.

Finally, thank you to my parents, Dale and Janeel Burningham, for their unconditional love and support.

CHAPTER 1

INTRODUCTION

The concept and theory behind prestressed concrete have been around for over 100 years. In this short time, prestressed concrete applications have become commonplace in structural engineering projects. Prestressed concrete can be found in bridges, underground structures, parking garages, power generation facilities, offshore oil rigs, and buildings. Advancements in materials such as development of high strength steel, increased compressive strength in concrete, as well as the development of design methods implementing high strength steel have promoted prestressed concrete to the popular status it enjoys today.

The act of prestressing concrete introduces a longitudinal compressive prestressing force into the structural member not found in conventional reinforced concrete. This prestressing force creates camber, reduces tensile stresses in the concrete, reduces and prevents cracks from forming, and reduces deflections. Such advantages come with increased cost due to the need for higher quality materials, more complicated formwork, and the additional cost of prestressing equipment; however, prestressed concrete produces a more economical long-term solution due to a longer design life (when the tendons and anchorage do not corrode), reduced maintenance frequency, decreased structure weight, and increased quality control.

The benefit of modern prestressed concrete is dependent on the use of high strength steel tendons to apply the prestressing force. There are two methods of introducing a prestressing force. The first method involves stressing the tendons in the framework, placing the concrete, curing the concrete, and releasing the stress in the tendons by cutting them flush with the concrete surface when the formwork is removed. As the tendons contract within the hardened concrete, the prestressing force is distributed into the restraining concrete member. The second method involves post-tensioning the high strength tendons in preplaced ducts after the concrete has been cast and has reached a specified strength. The high strength tendons are stressed and anchored at the ends of the member in order to maintain and distribute the prestressing force to the concrete. The research in this dissertation is limited to concrete beams with external post-tensioned CFRP composite tendons.

Current practice for post-tensioning depends on high strength steel tendons. Steel is readily available, but is susceptible to corrosion. If the steel tendons (or anchors) corrode, tendon failure may occur, rendering the structure unsafe for service loads. This potential loss of strength due to corrosion results in a decreased lifespan and increased cost as structures need to be replaced more frequently. Another contributor to the increased cost of post-tensioning is the need for large hydraulic jacks to stress the tendons. These jacks require several feet of space behind a concrete element in order to be able to apply the post-tensioning force—a major impediment in repair and rehabilitation applications. Additionally, the weight of a hydraulic jack requires the use of lifting equipment, such as a crane, to place, support, and move the jack from tendon to

tendon. Improvements in tendon materials and the method of stressing tendons can result in decreased life cycle cost and savings in construction time and cost.

One such material with potential to improve post-tensioning for repair and rehabilitation applications is fiber reinforced polymer (FRP) composites. Carbon fiber reinforced polymer (CFRP) materials are lighter than steel, have a comparable strength, and are not susceptible to metal corrosion. These characteristics result in a reduced labor cost for tendon placement and a reduced life cycle cost because the tendons do not corrode. Furthermore, improvements in the method of stressing CFRP tendons would also result in decreased cost and increased efficiency.

Implementation of cost advantageous FRP materials is not limited to new construction. FRP tendons can be used in rehabilitation and repair applications for structures that were under-designed, have become damaged through corrosion or overload, or structures for which increased capacity is desired. The application in repair and rehabilitation scenarios is a promising use of FRP post-tensioning (Täljsten and Nordin 2007). Additionally, although there is potential for a wide range of applications, widespread industry implementation and use of post-tensioned FRP tendons in repair and rehabilitation applications is contingent on overcoming three barriers. These three barriers are as follows:

1) lack of a simple, economical anchor that controls slip and adequately grips FRP tendons without unduly compromising the composite tendons;
2) need for an innovative stressing device that makes use of a single anchor setup and reduces the length of free space required behind a concrete member during post-tensioning; and

3) absence of standardized design guidelines detailing the use of FRP tendons, prediction of developed effective tendon stress, and placement of FRP tendons for the repair of concrete beams.

This dissertation presents research that overcomes the three aforementioned barriers, resulting in a contribution to the specialty of post-tensioned CFRP tendon applications in reinforced and prestressed concrete. The contributions can reduce cost, increase efficiency, promote industry acceptance of post-tensioned FRP tendons, and provide a means of repairing and retrofitting damaged structures. These contributions are detailed in subsequent chapters. Chapter 2 provides a literature review encompassing current anchors for use with FRP tendons, existing tendon stressing methods, and previous research on design methods for using FRP tendons with concrete members.

Chapter 3 describes the present research carried out to develop a unibody clamp anchor for prestressing CFRP rods. Details for four anchor generations are provided, including anchor design, application, laboratory testing, and experimental results. Additionally, a finite element analysis is presented and discussed to provide a relative comparison of the performance of the four anchor generations.

Chapter 4 details the application of the aforementioned unibody clamp anchors, CFRP rods, and a novel mechanical stressing device as a repair system for shear controlled normally reinforced concrete members. Features and aspects of the stressing process and stressing device are outlined, and an assessment of the success of the repair system is provided. Additionally, equations from the literature are evaluated for applicability to the specimens studied in the present research.

Chapter 5 focuses on the application of the CFRP repair system; however, the specimens considered are flexure controlled prestressed concrete beams. The chapter includes testing methods, specimen design and an analysis of the results—with an emphasis on the successful repair of the damaged specimens. In addition, equations from the literature typically applied to conventional steel prestressing tendons are evaluated to determine their applicability to the specimens considered in this research.

Finally, Chapters 6 and 7 contain an explanation and discussion of the conclusions generated by the entire research study and suggestions for future research, respectively.

1.1 References

Täljsten, B., and Nordin, H., 2007, "Concrete Beams Strengthened with External Prestressing Using External Tendons and Near-Surface-Mounted Reinforcement," ACI SP-245, pp. 143-164.

CHAPTER 2

LITERATURE REVIEW

The concept of using CFRP materials in post-tensioning applications is a relatively recent development. This literature survey will summarize the current state of knowledge regarding the use of fiber reinforced polymer (FRP) tendons in post-tensioned concrete. Additionally, the survey of available literature will identify some unsolved aspects relating to FRP tendons. Initially, the types of anchors used for FRP tendons will be reviewed. Next, the current methods of introducing a prestressing force into FRP tendons will be examined. Finally, contemporary design equations relating to the use of FRP tendons in post-tensioning applications will be presented.

2.1 FRP Anchorage

The anchor on a stressed tendon is paramount to the success of a post-tensioned system. The anchor must grip the FRP tendon such that slip is controlled and the tendon is not damaged during gripping. Damage can occur to the outer fibers of the tendon on the lead end (entrance end) of the anchor from stress concentrations. Damaged outer fibers decrease the overall capacity of the FRP tendon and can result in premature tendon failure. Thus, the focus during anchor design has been placed on mitigating the stress concentrations that may develop. Several types of anchors have been considered in

previous research studies; however, no single anchor has been shown to be simple, cost effective, easily manufactured, and still able to control slip and stress concentrations.

Clamping anchors have been developed using multiple metal blocks clamped together by bolts or spring elements. The blocks are clamped around the rod, and in some cases, a soft sleeve layer has been used between the FRP tendon and the clamp (Sippel 1992; Malvar and Bish 1995; Scheibe and Rostásy 1995). Plug and cone anchors used with traditional steel prestressing strands have also been applied to FRP tendons. This type of anchor involves seating a wedge into the end of the tendon such that the friction developed between the wedge, tendon fibers, and anchor sleeve holds the tendon securely (Malvar and Bish 1995). The plug and cone anchor has been most successful with FRP tendons containing no resin such as Parafil ropes (Burgoyne 1993). Another type of anchor, the resin sleeve anchor, has been successfully implemented to anchor FRP tendons (Reda Taha et al. 1994; Malvar and Bish 1995). This simple anchor consists of filling a sleeve of larger diameter than the FRP tendon with epoxy resin and allowing it to dry. A resin sleeve anchor is attractive because of the ability to generate bonding through its development length without inducing stress concentrations at the lead end of the anchor. However, to achieve this development length, a relatively long anchor is required.

The potted resin anchor is a modification of the resin sleeve anchor in that instead of implementing a constant diameter sleeve, a conical sleeve of varying diameter is used. It was has been shown that a cone with a parabolic shape works best (Holte et al. 1993). Additionally, metal overlay anchors have been used with FRP tendons. In this anchor, a

soft metal is placed over the tendon where the tendon will be gripped during jacking (Erki and Rizkalla 1993).

Finally, split wedge anchors have received the most attention. This is possibly due to the fact that split wedge anchors are commonly found in conventional high strength steel tendon anchors. This anchor works through split wedges being placed around the tendon, with the assembly then being placed in a conical shaped barrel. A soft sleeve may or may not be placed around the tendon before the wedges are installed. In some cases, it has been observed that a split wedge anchor can be used successfully without a sleeve (Al-Mayah et al. 2007). Several applications of this type of anchor have proved to have partial success (Hodhod and Uomoto 1992; Reda Taha 1994; Nanni et al. 1996; Sayed-Ahmed and Shrive 1998; Al-Mayah et al. 2001; Al-Mayah et al. 2005), and United States Patents with different variations have resulted (Meier et al. 1998; Shrive et al. 2000).

Furthermore, varying the number of wedges (2, 3, 4, and 6 wedges) has also been considered (Al-Mayah et al. 2001; Al-Mayah et al. 2007). Various wedge materials such as polymers (Kerstens et al. 1998; Täljsten and Nordin 2007; Terrasi et al. 2011), metal (Al-Mayah et al. 2001; Al-Mayah et al. 2005; Al-Mayah et al. 2007), and ultra high performance concrete (Reda Taha and Shrive 2003a, b) have been studied. Reported performance varies throughout the literature, but reducing the number of wedges used in the anchor reduces manufacturing costs (Al-Mayah et al. 2007). Split wedge anchors have been implemented to develop the ultimate strength of FRP tendons; however, slip was not necessarily controlled by the anchor (Nanni et al. 1996). Other split wedge anchors have failed to develop the ultimate strength of the FRP tendon due to increased stress concentrations in the radial direction of the tendon (Hodhod and Uomoto 1992).

This local damage to the tendon caused by the gripping anchor is the most common failure mode associated with split wedge anchors (Reda Taha and Shrive 2003a). Variations in the angle between the wedges and barrel (Sayed-Ahmed and Shrive 1998) and sleeve material (Al-Mayah et al. 2001) have shown that these factors are important to controlling slip and the contact pressure between the sleeve and the FRP tendon.

2.2 Methods of Stressing Tendons

The author has been unable to find any literature detailing a unique system for prestressing FRP tendons. Previous research involving concrete specimens with prestressed or post-tensioned FRP tendons have relied on traditional hydraulic jacking methods (Grace and Abdel-Sayed 1998; Ng 2005; El-Hacha and Elbadry 2006; Soudki and Ng 2007; Täljsten and Nordin 2007; Badawi and Soudki 2009). Often, the traditional method involves the use of two FRP tendon anchors per tendon at the stressing end. One anchor functions as the stop while the hydraulic jack pulls back on the anchor, and the second anchor is used to maintain the prestressing force in the tendon after the jack is released. Unfortunately, no data regarding the length of the jacking equipment or the required space behind the concrete specimens were reported. However, photographs from the literature suggest that a minimum of three feet is required behind the end of the specimen to complete the jacking process with a hydraulic jack. In field applications, the requirement for free space increases, and it is the author's estimate that at least five feet is required for prestressing conventional high strength steel tendons in full size concrete members.

2.3 Current Design Methods

Some studies have been performed to compare actual test data from concrete beams with external FRP tendons to analytical models. These studies have evaluated the applicability of various methods and design guidelines in determining the performance of concrete beams post-tensioned with FRP tendons. It has been found that the American Concrete Institute's Building Code Requirements for Structural Concrete—ACI 318—(ACI Committee 318 2008) produces an overly conservative prediction of the performance of beams with FRP tendons. Moreover, it has been shown that ACI-318 (ACI Committee 318 2008) results in acceptable predictions of shear cracking loads for beams with internal FRP tendons, but its use underestimates stirrup strain after shear cracks form. In contrast, the modified compression field theory was found to provide an acceptable prediction of specimen capacity (Fam et al. 1997). One study found that the strut-and-tie model provisions of ACI-318 (ACI Committee 318 2008) underestimated capacities observed in laboratory test specimens by more than 200% in some cases (Ng 2005; Soudki and Ng 2007).

Studies have also been done regarding the applicability of foreign design codes. One study found that for beams with unbonded FRP tendons, the cracking, yield, and ultimate flexural loads could be "roughly estimated" by the Architectural Institute of Japan's Prestressed Concrete Standards (Kato and Hayashida 1993). Additionally, research has been carried out to investigate the applicability of equations developed by ACI Committee 440, the Intelligent Sensing for Innovative Structures (ISIS) Canada Research Network, and the Comité Euro-International de Béton – Fédération International de la Précontrainte (CEB-FIP). Results showed that equations proposed by

ACI Committee 440 provided the most accurate predictions of the force in post-tensioned tendons. Additionally, all three equations were found to underestimate the "effective rigidity of the beam." (Abdel Aziz et al. 2005).

Other methods of analyzing specimens with FRP tendons include the consideration of strain reduction coefficients and a layer-by-layer analysis of beam cross sections. This method was found to result in "good agreement" between predicted and experimental results (Elrefai et al. 2007). Experimental results have also been compared to modified strut-and-tie models in which the strut is replaced by an arch band such that only one model exists for one beam (Ng 2005). A second model, based on a general arch model, was also considered in the same research. A comparison of experimental data and the predictions of the two aforementioned models suggested the models work well for the prediction of the ultimate capacity of shear controlled specimens incorporating post-tensioned CFRP tendons (Ng 2005; Soudki and Ng 2007). In addition, it has been suggested that methods for the prediction of flexural capacity using stresses developed in unbonded high strength steel tendons are also applicable to unbonded FRP tendons (Naaman et al. 2002).

2.4 References

Abdel Aziz, M.; Abdel-Sayed, G.; Ghrib, F.; Grace, N.; and Madugula, M., 2005, "Analysis of Concrete Beams Prestressed and Post-Tensioned with Externally Unbonded Carbon Fiber Reinforced Polymer Tendons," *Canadian Journal of Civil Engineering*, V. 31, pp. 1138-1151.

ACI Committee 318, 2008, "Building Code Requirements for Reinforced Concrete (ACI 318-08) and Commentary (ACI 318R-08)," American Concrete Institute, Farmington Hills, MI.

Al-Mayah, A.; Soudki, K.; and Plumtree, A., 2001, "Mechanical Behavior of CFRP Rod Anchors Under Tensile Loading," *Journal of Composites for Construction*, V. 5, pp. 128-135.

Al-Mayah, A.; Soudki, K.; and Plumtree, A., 2007, "Simplified Wedge Anchor System for FRP Rods," *FRPRCS-8*, Patras, Greece.

Al-Mayah, A.; Soudki, K.; and Plumtree, A., 2005, "Variable Thickness Barrel Anchor for CFRP Prestressing Rods," *Ned Burns Symposium on Historic Innovations in Prestressed Concrete*, ACI SP-231, pp. 237-252.

Badawi, M., and Soudki, K., 2009, "Flexural Strengthening of RC Beams with Prestressed NSM CFRP rods—Experimental and Analytical Investigation," *Construction and Building Materials*, V. 23, pp. 3292-3300.

Burgoyne, C., 1993, "Parafil Ropes for Prestressing Applications," *Fibre-Reinforced Plastic (FRP) for Concrete Structures: Properties and Applications*, Elsevier Science, New York, NY, pp. 333-351.

El-Hacha, R., and Elbadry, M., 2006, "Strengthening Concrete Beams With Externally Prestressed Carbon Fiber Composite Cables: Experimental Investigation," *PTI Journal*, V. 4, No. 2, pp. 53-70.

Elrefai, A.; West, J.; and Soudki, K., 2007, "Strengthening of RC Beams with External Post-Tensioned CFRP Tendons," ACI SP-245-8, pp. 123-142.

Erki, M., and Rizkalla, S., 1993, "Anchorage for FRP Reinforcement," *Concrete International*, V. 15, No. 6, pp. 54-59.

Fam, A.; Rizkalla, S.; and Tadros, G., 1997, "Behavior of CFRP for Prestressing and Shear Reinforcements of Concrete Highway Bridges," *ACI Structural Journal*, V. 94, No. 1, pp. 77-86.

Grace, N.; and Abdel-Sayed, G., 1998, "Behavior of Externally Draped CFRP Tendons in Prestressed Concrete Bridges," *PCI Journal*, Sept.-Oct., pp. 88-101.

Hodhod, H.; and Uomoto, T., 1992, "Effect of State of Stress at the Grips and Matrix Properties on Tensile Strength of CFRP Rods," *Japan Society of Civil Engineers*, V. 17, No. 451, pp. 245-252.

Holte, L.; Dolan, C.; and Schmidt, R., 1993, "Epoxy Socketed Anchors for Non-Metallic Prestressing Tendons," *Fibre-Reinforced-Plastic Reinforcement for Concrete Structures, International Symposium*, ACI SP-138, pp. 381-400.

Kato, T.; and Hayashida, N., 1993, "Flexural Characteristics of Prestressed Concrete Beams with CFRP Tendons," ACI SP-138-26, pp. 419-440.

Kerstens, J.; Bennenk, W.; and Camp, W., 1998, "Prestressing with Carbon Composite Rods: A Numerical Method for Developing Reusable Prestressing Systems," *ACI Structural Journal*, V. 95, No. 1, pp. 43-50.

Malvar, L., and Bish, J., 1995, "Grip Effects in Tensile Testing of FRP Bars," *Proceedings of the 2nd International RILEM Symposium (FRPRCS-2)*, London, pp. 108-115.

Meier, U.; Meier, H.; and Kim, P., 1998, "Anchorage Device for High-Performance Fiber Composite Cables," Patent No. 5,713,169, United States of America.

Naaman, A.; Burns, N.; French, C.; Gamble, W.; and Mattock, A., 2002, "Stresses in Unbonded Prestressing Tendons at Ultimate: Recommendation," *ACI Structural Journal*, V. 99, No. 4, pp. 518-529.

Nanni, A.; Bakis, C.; O'Neil, E.; and Dixon, T., 1996, "Performance of FRP Tendon-Anchor Systems for Prestressed Concrete Structures," *PCI Journal*, V. 41, No. 1, pp. 34-44.

Ng, S., 2005, "Shear Behaviour of RC Beams Externally Prestressed with CFRP Rods," Master's thesis, University of Waterloo, Waterloo, Ontario.

Reda Taha, M., and Shrive, N., 2003a, "New Concrete Anchors for Carbon Fiber-Reinforces Polymer Post-Tensioning Tendons-Part 1: State-of-the-Art Review/Design," *ACI Structural Journal*, V. 100, No. 1, pp. 86-95.

Reda Taha, M., and Shrive, N., 2003b, "New Concrete Anchors for Carbon Fiber-Reinforced Polymer Post-Tensioning Tendons-Part 2: Development/Experimental Investigation," *ACI Structural Journal*, V. 100, No. 1, pp. 96-104.

Reda Taha, M.; Sayed-Ahmed, E.; and Shrive, N., 1994, "Towards a New Non-Metallic Anchorage System for Post-tensioned Applications with Carbon Fiber Reinforced Plastic Tendons," *42nd International SAMPE Symposium*, Anaheim, CA, pp. 288-297.

Sayed-Ahmed, E., and Shrive, N., 1998, "A New Steel Anchorage System for Post-tensioned Applications with Carbon Fiber Reinforced Plastic Tendons," *Canadian Journal of Civil Engineering*, V. 25, No. 1, pp. 113-127.

Scheibe, M., and Rostásy, F., 1995, "Aspects of Laboratory Testing to Determine Mechanical Properties of FRP," *Proceedings of the 2nd International PILEM Symposium (FRPRCS-2)*, London, pp. 116-123.

Shrive, N.; Sayed-Ahmed, E.; Damson, E.; Tilleman, D.; and Tadros, G., 2000, Patent No. 6,082,063, United States of America.

Sippel, T., 1992, "Design, Testing, and Modeling of an Anchorage System for Resin Bonded Fiberglass Rods Used as Prestressing Tendons," *Advanced Composite Materials and Structures*, Sherbrooke, Quebec, pp. 363-372.

Soudki, K., and Ng, S., 2007, "Shear Behavior of RC Beams with External CFRP Prestressing Tendons," *FRPRCS-8*. Patras, Greece, 8 pp.

Täljsten, B., and Nordin, H., 2007, "Concrete Beams Strengthened with External Prestressing Using External Tendons and Near-Surface-Mounted Reinforcement," ACI SP-245, pp. 143-164.

Terrasi, G. P.; Affolter, C.; and Barbezat, M., 2011, "Numerical Optimization of a Compact and Reusable Pretensioning Anchorage System for CFRP Tendons," *Journal of Composites for Construction*, V. 12, No. 2, pp. 126-135.

CHAPTER 3

UNIBODY CLAMP ANCHORS FOR PRESTRESSING CFRP RODS

Clayton A. Burningham, Chris P. Pantelides, and Lawrence D. Reaveley

Clayton A. Burningham is a PhD candidate in the department of Civil and Environmental Engineering at the University of Utah. He received his bachelor's and MS degrees from the University of Utah. His research interests include repair of reinforced and prestressed concrete structures and post-tensioning CFRP materials.

ACI member **Chris P. Pantelides** is a Professor and Associate Chair of Civil and Environmental Engineering at the University of Utah. He received his bachelor's degree from the American University of Beirut and his MS and PhD from the University of Missouri-Rolla. His research interests include the seismic design, evaluation, and rehabilitation of reinforced concrete buildings and bridges.

Lawrence D. Reaveley is a Professor and former Department Chair of Civil and Environmental Engineering at the University of Utah. He received his bachelor's and MS degrees from the University of Utah and his PhD from the University of New Mexico. His research interests include structural dynamics with an emphasis on earthquake engineering, vibration problems, and seismic rehabilitation.

(To be submitted for publication)

3.1 Abstract

This paper presents research regarding four generations of unibody steel clamp anchors for prestressing CFRP rods. Geometric properties and bolts used to provide the clamping force were varied across the four anchor generations. The anchors performed well, and generation IV performed the best with an anchor efficiency of 84% based on the manufacturer specified ultimate strength. Additionally, results from ANSYS finite element models are discussed. The results provide a relative comparison of the contact pressure between the anchor and CFRP rod across the four generations. Generation IV was found to provide the highest contact pressure while controlling stress concentrations at the lead (load) edge of the anchor.

Keywords: CFRP, composites, prestressing, clamp anchor, post-tensioning

3.2 Introduction

Post-tensioned concrete is conventionally constructed with high strength steel tendons. An attractive alternative to steel tendons is fiber reinforced polymer (FRP) tendons due to their high strength-to-weight ratio, corrosion resistance, and resistance to fatigue. As with high strength steel tendons, FRP tendons must also have proper anchorage for post-tensioning to occur. Because the success of implementing FRP materials in post-tensioning applications depends on the anchors, much consideration should be given to developing a suitable anchor.

Some research has been performed on several different styles of anchors for prestressing applications of FRP tendons (Nanni et al. 1996). Common considerations for the development of FRP anchors include efficiency, stress concentrations, economics, and corrosion resistance. Concerns regarding stress concentrations are directly related to

the anchor efficiency; transversely isotropic FRP tendons can prematurely fail if the transverse stress is not controlled, especially at the leading edge of the anchor. An acceptable anchor for FRP tendons must ensure that rupture of the FRP tendon occurs outside of the anchorage (Meier et al. 1998). On the other hand, the anchor must sufficiently retain the tendon through an applied stress such that slip does not occur during the tendon stressing application or subsequent time in service. Additionally, economics must be considered in anchor design because although an anchor is proven with laboratory research, an exorbitant unit cost would be prohibitive to industry acceptance. Finally, corrosion resistance must be considered because the anchor system should be able to meet the performance life of the highly corrosion resistant FRP tendon.

Anchors for FRP tendons fall into one of two broad categories based on the method employed for imparting stress to the FRP tendon: bond anchors and mechanical anchors (Reda Taha and Shrive 2003a). Generally composed of a sleeve filled with resin, bond anchors rely on the bond between the resin and the FRP tendon to provide adequate contact pressure during prestressing or post-tensioning applications. Different styles of bond anchors may include a tapered or conical sleeve, splayed ends of the FRP tendon, or tendon overlay materials. Bond anchors have been developed for use with FRP tendons (Malvar and Bish 1995; Reda Taha, et al. 1994; Holte, et al. 1993); however, largely dependent on development length, bond anchors tend to be longer than mechanical anchors—making them less practical where end anchorage must be compact. Additionally, the dependency on resin or epoxy of bond anchors results in increased application time, labor costs, and possibility of installation error.

Mechanical anchors are typically classified as wedge anchors or clamp anchors. Split wedge anchors are similar to anchors used for prestressing conventional high strength steel tendons, and consist of wedges that surround the FRP tendon and a conical barrel outside the wedges. As stress is applied to the tendon, the wedges are seated into the barrel, applying a gripping stress to the tendon. Additionally, a soft sleeve material around the tendon may or may not be included with split wedge anchors to attempt to reduce transverse stress concentrations. The number of wedges has been investigated, with variations of 2, 3, 4, and 6 wedges (Al-Mayah et al. 2007; Al-Mayah et al. 2001). Different wedge materials have also been studied. Tests have been conducted on high performance concrete anchors (Reda Taha and Shrive 2003a; Reda Taha and Shrive 2003b), polymer anchors (Täljsten and Nordin 2007; Kerstens et al. 1998; Terrasi et al. 2011), and metal anchors (Al-Mayah et al. 2007; Al-Mayah et al. 2001; Al-Mayah et al. 2005). Although split wedge anchors have been implemented in laboratory testing to develop the ultimate strength of the tendon, slip has not always been controlled (Nanni et al. 1996). Other split wedge anchors have failed to develop the ultimate strength of the tendon due to increased transverse stresses (Hodhod and Uomoto 1992). It is of note that although split wedge anchors are compact, they can have a higher manufacturing cost than bond anchors due to the number of wedges and the machining required to produce the precise tapers and angles for the wedges and barrel.

Clamp anchors impart a mechanical stress to the FRP tendon from bolts or similar mechanical devices rather than wedges being driven into a barrel. Traditionally composed of two metal plates with a groove for the FRP tendon, clamp anchors can be more compact than bond anchors, and in some cases, a sleeve material has been used between

the tendon and the clamp (Malvar and Bish 1995; Sippel 1992; Scheibe and Rostásy 1995). Clamp anchors generally have lower manufacturing costs than split wedge anchors because less machining is required. Despite the research investigations of various types of FRP tendon anchors, no single type has found widespread acceptance or implementation in industry.

As such, clamp anchors are especially suited for overcoming the limitations of other anchor systems. Manufacturing costs for clamp anchors are lower than those for split wedge anchors because less machining is required, and fewer pieces are involved in the anchor assembly. Additionally, clamp anchors are more compact than bond anchors because the clamping force applied can be adjusted with the bolts, reducing the development length required. Furthermore, the applied stress can be varied along the anchor to control transverse stresses and avoid premature FRP tendon failure. Stainless steel could be used for the anchor, and it is also of note that a clamp anchor can be further simplified if a unibody design is implemented, thus reducing the number of parts and field application time.

The research in this paper presents groundwork design of a unibody clamp anchor for prestressing CFRP rods. Details of the anchors, anchor application, laboratory testing, and results are provided. Additionally, a finite element analysis of the relative performance between four anchor generations is presented and discussed. Finally, recommendations for further development of clamp anchor systems are presented.

3.3 Research Significance

Although research has focused on several types of anchors for use with prestressing FRP rods, no single type or design has been widely accepted or implemented

in the industry. Efficiency, economics, control of anchor slip, and transverse stresses have been the primary challenges in successful anchor development. This research seeks to overcome the aforementioned challenges with a unibody clamp anchor. Design considerations addressing the challenges are presented and discussed. Additionally, a finite element model is used to provide a relative comparison between four generations of the anchor to investigate the improvement in clamping action. Furthermore, because the unibody anchor in this research overcomes many of the challenges associated with previous anchors for FRP tendons, it could lead to the widespread application of CFRP post-tensioning systems in industry for both new and repair applications.

3.4 Experimental Investigation

3.4.1 Specimen Geometry

Four unique generations of unibody anchors were studied in this research, and the generalized geometry of the unibody clamp anchor developed in this research can be seen in Fig. 3.1. All four generations were composed of a steel block of 1018 cold-rolled flat bar with a rod hole, bolt holes, an inner slot, and an outer slot. The rod hole is positioned longitudinally along the anchor block with the inner and outer slots running parallel to the rod hole. Additionally, the bolt holes and bolts run perpendicular to the rod to provide the clamping force. Therefore, as the bolts are tightened, the outer and inner slot widths are reduced and the cantilevered anchor sides are pushed inward—resulting in contact pressure on the CFRP rod. The width of inner and outer slots controls the effects of the bolt tension; once either slot is completely closed, an increase in bolt force simply deforms the steel of the anchor while negligibly increasing the clamping pressure applied to the CFRP rod. Variables such as anchor length, width, and thickness were varied

across generations; a summary of the anchor geometry for each generation can be seen in Table 3.1. A visual size comparison of the anchors across the four generations can be seen in Fig. 3.2.

Another variation between generations was implemented by varying the number and size of the A325 steel bolts used to apply the clamping force. A summary of the variation in the bolts used for each anchor generation can be seen in Table 3.2. The bolt diameters for generations I-III and generation IV were 5/8” (16 mm) and 3/4” (19 mm), respectively. Additionally, generation I utilized two bolts, generation II three bolts, and generations III and IV four bolts with the bolt spacing held constant at 1.5 in. (38.1 mm). The applied torque for each bolt varied across generations; however, each bolt in a given anchor was subjected to the same applied torque.

3.4.2 Material Properties

The material used in the manufacture of the unibody anchors was1018 cold rolled flat bar with a minimum yield strength of 53.8 ksi (371 MPa), and the clamping force was provided by A325 steel bolts. Additionally, the CFRP rods used in this research had the following design properties as provided by the manufacturer: rod diameter = 3/8 in. (9.53 mm), tensile strength = 27.5 kip (122.3 kN), tensile modulus = 22,500 ksi (155 GPa), and elongation at break = 1.1%.

3.4.3 Testing Methods

The unibody clamp anchors were tested in the University of Utah Structural Testing Laboratory. A length of CFRP rod was prepared to include the length of the anchor sections, the middle section, and a short 1 in. (25 mm) nub protruding from the dead end of each anchor such that the total length was longer than 40 times the diameter

of the CFRP rod, which is 15 in. (381 mm), as per ACI 440.3R-04 (ACI Committee 440 2004). A blended liquid solvent was used to clean the anchors and CFRP rod test sections before clamping occurred.

Anchor clamping was accomplished with steel bolts. Each bolt was secured sequentially, beginning with the dead end of the anchor and progressing towards the lead end. The clamping process occurred over several increments until the final applied torque (as described later) was reached for each bolt. Additionally, generations III-IV included the use of tapered drop forged steel washers to ensure the clamping bolts remained perpendicular to the anchor. An example photograph showing the implementation of the tapered washers can be seen in Fig. 3.3. A matching anchor was clamped to each end of a given CFRP rod test section, creating a test section assembly.

After application of the unibody clamp anchors, the test section assemblies were tested vertically. The bottom clamp anchor was held in fixed position by a slotted steel reaction plate while a tensile force was applied to the test section assembly at the top clamp anchor by a hydraulic actuator, as seen in Fig. 3.4. Monotonic loading was applied at a rate of 0.4 in./min (10.2 mm/min), which corresponds to an idealized stress application rate of 60 ksi/min (414 MPa/min). Termination of each test was dependent on rupture of the CFRP rod or more than 0.5 in. (13 mm) of total anchor slip, whichever occurred first.

3.5 Experimental Results

3.5.1 Generation I Anchor

The first generation anchor can be seen in Fig. 3.5. This was the shortest of the four generations at 3.0 in. (76 mm) long, and the clamping force was provided by two 5/8

in. (16 mm) diameter A325 bolts. Figure 3.6 shows typical results from a generation I anchor. An anchor without slip would result in a perfectly linear relationship between applied force and actuator displacement. It can be seen from Fig. 3.6 that typical generation I anchors reached a maximum load of 17 kip (75.6 kN), corresponding to an anchor efficiency of 62% based on the manufacturer specified ultimate strength before slip occurred. For loads greater than 17 kip (75.6 kN), large amounts of slip were present, as indicated by the curvature of the plot seen in Fig. 3.6. The CFRP rod remained intact during testing; however, the slip of the anchor on the rod produced a scaling effect on the CFRP rod, which is visible in Fig. 3.7. Additionally, as seen in Fig. 3.5, it was observed that the 3/16 in. (4.8 mm) constant width outer slot limited the maximum clamping force due to contact occurring between the steel surfaces at the outer edges of the outer slot. Furthermore, bolt failure occurred because the bolts bent during the clamping process and did not remain perpendicular to the anchor.

3.5.2 Generation II Anchor

The second generation anchor improved upon the previous generation by increasing the anchor length to 4.5 in. (114 mm) and using three bolts to provide the clamping force. The closed outer slot of a typical clamped generation II anchor can be seen in Fig. 3.8. Typical results from testing of a generation II anchor can be seen in Fig. 3.9. Generation II anchors exhibited linear performance up to a maximum load of 20 kip (89.0 kN), corresponding to an anchor efficiency of 73% based on the manufacturer specified ultimate strength before slip occurred. At applied tensile loads greater than 20 kip (89.0 kN), some slip was observed and the CFRP rod underwent progressive failure—the outer fibers ruptured first and moved inward towards the center of the rod.

Rod failure occurred near the lead end of the anchor as seen in Fig. 3.10. Therefore, although the clamping force was limited—as with generation I—the increase in anchor length reduced the observed slip and resulted in increased anchor efficiency for generation II as compared to generation I. However, despite the increased anchor efficiency, bolt bending was observed during the clamping process.

3.5.3 Generation III Anchor

Modifications to produce generation III included increasing the anchor length to 6.0 in. (152 mm) and using four 5/8 in. (16mm) diameter bolts to control anchor slip. Additionally, tapered washers were used to ensure the clamping bolts remained perpendicular to the anchor during the clamping process. Figure 3.11 shows typical test results from a generation III anchor. From Fig. 3.11, it can be seen that generation III anchors reached a maximum load of 22 kip (97.9 kN) before slip occurred, corresponding to an anchor efficiency of 80% based on the manufacturer specified ultimate strength. The total anchor slip above this tensile load was observed to be only 0.01 in. (0.254 mm). Additionally, the failure of the CFRP rod occurred instantaneously in the middle of the test section, resulting in flared strands at the midpoint of the CFRP rod, as seen in Fig. 3.12. Compared to the results of the previous generation, generation III exhibited less anchor slip, and rod rupture occurred in the middle of the test section rather than at the lead edge of the anchors. It was also observed that the tapered washers ensured that the bolts remained perpendicular to the anchor and did not bend during the clamping process.

3.5.4 Generation IV Anchor

Generation IV included an increase in anchor length (at the lead edge), anchor thickness, and clamping bolt diameter. Additionally, an outer slot of varying width

(corresponding to an approximate 5 degree taper) was implemented, as seen in Fig. 3.13. The tapered outer slot ensured contact did not occur between the edges of the outer slot—allowing for an increase in applied clamping force. Furthermore, as with generation III, tapered washers were utilized to maintain the clamping bolts perpendicular to the anchor. A clamped generation IV anchor can be seen in Fig. 3.14. Typical test results from a generation IV anchor can be seen in Fig. 3.15. From Fig. 3.15 it can be seen that generation IV anchors exhibited acceptable performance for the entire test; no anchor slip was observed. The CFRP rod failed at a maximum load of 23 kip (102.3 kN), corresponding to a true anchor efficiency of 84% based on the manufacturer specified ultimate strength. Although the bolt spacing for generations III and IV remained constant, the extra anchor length of generation IV was added to the anchor lead edge to gradually reduce the pressure exerted by the anchor on the CFRP rod. This effect is evidenced by the gradual flare in the outer slot width observed in Fig. 3.14—where the slot is wider on the right side as compared to the left side. Additionally, the bolts did not bend because of the use of the tapered washers.

3.6 Finite Element Modeling

3.6.1 Model Configuration

In addition to laboratory testing, a finite element model was developed in ANSYS for all four anchor generations to explore the relative difference in clamping pressure between generations. Tetrahedral elements were selected for the convenience of automatic meshing, and full 3D models were developed due to the complexity of the variations between anchor generations. The ANSYS geometry and mesh for generation IV can be seen in Fig. 3.16. Due to the intensive nature of full 3D modeling, the unibody

steel anchor was modeled using a simple bilinear stress-strain relationship to reduce the overall computational time. Additionally, the CFRP rod was modeled as a transversely isotropic material with different properties in the longitudinal direction as compared to the transverse direction.

The contact between the unibody steel anchor and CFRP rod was modeled with contact and target elements overlaid on the CFRP rod and anchor surfaces, respectively. Models for generations I-III included additional contact and target elements on the inner surfaces of the outer slot since contact was expected to occur at the edges of the outer slot as observed during laboratory testing. Additionally, the nature of the unibody clamp anchors studied in this research is such that a contact pressure is developed from the clamping force provided from bolts rather than a seating force as with split wedge anchors. Therefore, for the purposes of investigating the relative difference in contact pressure across the four unibody anchor generations, a clamping force was applied, but no tensile force was modeled in the CFRP rod.

The modeled force in each bolt was input as 12.0 kip (53.4 kN) and 13.4 kip (59.6 kN) for generations I-III and generation IV, respectively. These bolt forces were calibrated to produce deflections in the ANSYS model corresponding to deflections in the anchors observed during the experimental clamping process.

3.6.2 Model Results

Results from the ANSYS models confirm the results from laboratory testing—generation IV reduces stress concentrations at the lead edge of the anchor and produces the highest contact pressure of the four generations studied. A nub end view of the generation IV model showing the deflected shape and equivalent stress can be seen in

Fig. 3.17; the tapered outer slot has essentially become a slot of constant width, as observed in laboratory testing. The effect of the clamping process can be seen when comparing Fig. 3.13 to Fig. 3.17. Additionally, the reduction in stress in the CFRP rod at the lead (load) edge of the generation IV anchor can be seen in Fig. 3.18. From the cross section view in Fig. 3.18 it is observed that the equivalent stress in the CFRP rod is much higher at the nub (left) end as compared to the lead (right) end. This is due to the additional length of steel at the lead end provided in generation IV and as also seen in Fig. 3.18.

The reduction in contact pressure and subsequently stress in the CFRP rod at the lead edge of the anchor is further illustrated in Fig. 3.19 which shows the change in clamping pressure on the side of the CFRP rod along the length of the anchor for generations I-IV. It can be seen from Fig. 3.19 that generations I-III provide approximately the same contact pressure along the entire anchor length. In contrast, the generation IV anchor exhibits an increase in contact pressure of approximately 60% (compared to generations I-III), and at the same time, a gradual 37% decrease in contact pressure towards the lead edge. This decrease in contact pressure indicates that the geometric design of generation IV is able to reduce the contact pressure and subsequent stress concentrations in the CFRP rod at the lead edge. Furthermore, the varying width of the outer slot in generation IV allows for an increase in the overall contact pressure because the edges of the outer slot are prevented from touching. Therefore, although improvement can be seen from generations I-III in terms of development length, the best unibody clamp anchor considered in this research is the generation IV anchor because of

its ability to reduce the stress concentrations at the lead anchor edge and its ability to apply a higher clamping force as compared to generations I-III.

3.7 Conclusions

From the experiments carried out in this research and the ANSYS finite element model results, it can be concluded that the unibody clamp anchors studied in this research can be used for prestressing or post-tensioning CFRP rods. The simple geometry is absent of complicated wedges, bevels, and multiple pieces. The generation IV anchor was found to perform the best. Based on the manufacturer specified ultimate strength, anchor generations I-III demonstrated an anchor efficiency before slip of 62%, 73%, and 80%, respectively. The generation IV anchors demonstrated an anchor efficiency of 84% before CFRP rod rupture.

In addition to increased anchor efficiency, the inclusion of extra length at the load or lead end of the anchor (where the CFRP rod leads out of the anchor to the other end of the CFRP rod) was found to produce a 37% reduction of the contact pressure at the lead edge of the generation IV anchor. Furthermore, the tapered outer slot included in the generation IV anchor allowed for an increased clamping force as compared to other generations because it prevented the edges of the outer slot from touching.

It is recommended that future studies be carried out to optimize the design of the generation IV anchor to increase the anchor efficiency. It is anticipated that further reducing the contact pressure at the lead edge of the anchor will contribute to the anchor optimization. Variables such as anchor thickness and length should be explored in the optimization process. Additionally, the effect of varying the applied torque to each bolt in the anchor should be investigated. It is possible the effect of adding extra anchor length to

the lead end may be replicated by simply reducing the torque applied to the lead bolt. This exploration is essential as any reduction in anchor length would be beneficial for repair applications where space for anchorage is limited.

Future iterations should ensure that anchor slip does not occur while minimizing anchor length. Additionally, it is recommended that future studies implement the unibody clamp anchor to prestress CFRP rods on reinforced concrete specimens, simulating field applications. Furthermore, stainless steel should be explored as an option for the anchor stock and bolts to prevent corrosion.

3.8 Acknowledgements

The authors wish to acknowledge the assistance of Mark Bryant and Mike Gibbons in specimen fabrication and testing. Additionally, the authors wish to thank Uma Ramasamy, Brett Raddon, and Tyler Ross for their guidance with finite element modeling.

3.9 References

ACI Committee 440, 2004, "Guide Test Methods for Fiber-Reinforced Polymers (FRPs) for Reinforcing or Strengthening Concrete Structures (ACI 440.3R-04)," American Concrete Institute, Farmington Hills, MI.

Al-Mayah, A.; Soudki, K.; and Plumtree, A., 2001, "Mechanical Behavior of CFRP Rod Anchors Under Tensile Loading," *Journal of Composites for Construction*, V. 5, pp. 128-135.

Al-Mayah, A.; Soudki, K.; and Plumtree, A., 2007, "Simplified Wedge Anchor System for FRP Rods," *FRPRCS-8*, Patras, Greece.

Al-Mayah, A.; Soudki, K.; and Plumtree, A., 2005, "Variable Thickness Barrel Anchor for CFRP Prestressing Rods," *Ned Burns Symposium on Historic Innovations in Prestressed Concrete,* ACI SP-231, pp. 237-252.

Hodhod, H.; and Uomoto, T., 1992, "Effect of State of Stress at the Grips and Matrix Properties on Tensile Strength of CFRP Rods," *Japan Society of Civil Engineers*, V. 17, No. 451, pp. 245-252.

Holte, L.; Dolan, C.; and Schmidt, R., 1993, "Epoxy Socketed Anchors for Non-Metallic Prestressing Tendons," *Fibre-Reinforced-Plastic Reinforcement for Concrete Structures, International Symposium*, ACI SP-138, pp. 381-400.

Kerstens, J.; Bennenk, W.; and Camp, W., 1998, "Prestressing with Carbon Composite Rods: A Numerical Method for Developing Reusable Prestressing Systems," *ACI Structural Journal*, V. 95, No. 1, pp. 43-50.

Malvar, L., and Bish, J., 1995, "Grip Effects in Tensile Testing of FRP Bars," *Proceedings of the 2nd International RILEM Symposium (FRPRCS-2)*, London, pp. 108-115.

Meier, U.; Meier, H.; and Kim, P., 1998, "Anchorage Device for High-Performance Fiber Composite Cables," Patent No. 5,713,169, United States of America.

Nanni, A.; Bakis, C.; O'Neil, E.; and Dixon, T., 1996, "Performance of FRP Tendon-Anchor Systems for Prestressed Concrete Structures," *PCI Journal*, V. 41, No. 1, pp. 34-44.

Reda Taha, M., and Shrive, N., 2003a, "New Concrete Anchors for Carbon Fiber-Reinforces Polymer Post-Tensioning Tendons-Part 1: State-of-the-Art Review/Design," *ACI Structural Journal*, V. 100, No. 1, pp. 86-95.

Reda Taha, M., and Shrive, N., 2003b, "New Concrete Anchors for Carbon Fiber-Reinforced Polymer Post-Tensioning Tendons-Part 2: Development/Experimental Investigation," *ACI Structural Journal*, V. 100, No. 1, pp. 96-104.

Reda Taha, M.; Sayed-Ahmed, E.; and Shrive, N., 1994, "Towards a New Non-Metallic Anchorage System for Post-tensioned Applications with Carbon Fiber Reinforced Plastic Tendons," *42nd International SAMPE Symposium*, Anaheim, CA, pp. 288-297.

Scheibe, M., and Rostásy, F., 1995, "Aspects of Laboratory Testing to Determine Mechanical Properties of FRP," *Proceedings of the 2nd International PILEM Symposium (FRPRCS-2)*, London, pp. 116-123.

Sippel, T., 1992, "Design, Testing, and Modeling of an Anchorage System for Resin Bonded Fiberglass Rods Used as Prestressing Tendons," *Advanced Composite Materials and Structures*, Sherbrooke, Quebec, pp. 363-372.

Täljsten, B., and Nordin, H., 2007, "Concrete Beams Strengthened with External Prestressing Using External Tendons and Near-Surface-Mounted Reinforcement," ACI SP-245, pp. 143-164.

Terrasi, G. P.; Affolter, C.; and Barbezat, M., 2011, "Numerical Optimization of a Compact and Reusable Pretensioning Anchorage System for CFRP Tendons," *Journal of Composites for Construction*, V. 12, No. 2, pp. 126-135.

Table 3.1 – Anchor geometry details

Generation	Width	Length	Thickness	Inner Slot Width	Minimum Outer Slot Width	Maximum Outer Slot Width
I	2.0” (51 mm)	3.0” (76 mm)	1.0” (25 mm)	1/16” (1.6 mm)	3/16” (4.8 mm)	3/16” (4.8 mm)
II	2.0” (51 mm)	4.5” (114 mm)	1.0” (25 mm)	1/16” (1.6 mm)	3/16” (4.8 mm)	3/16” (4.8 mm)
III	2.0” (51 mm)	6.0” (152 mm)	1.0” (25 mm)	1/16” (1.6 mm)	3/16” (4.8 mm)	3/16” (4.8 mm)
IV	2.25” (57 mm)	6.5” (165 mm)	1.5” (38 mm)	1/16” (1.6 mm)	3/16” (4.8 mm)	13/16” (20.6 mm)

Table 3.2 – Clamping bolt details

Generation	Number of Bolts	Bolt Diameter	Applied Torque
I	2	5/8” (16 mm)	200 ft-lb (271 N-m)
II	3	5/8” (16 mm)	200 ft-lb (271 N-m)
III	4	5/8” (16 mm)	200 ft-lb (271 N-m)
IV	4	3/4” (19 mm)	600 ft-lb (813 N-m)

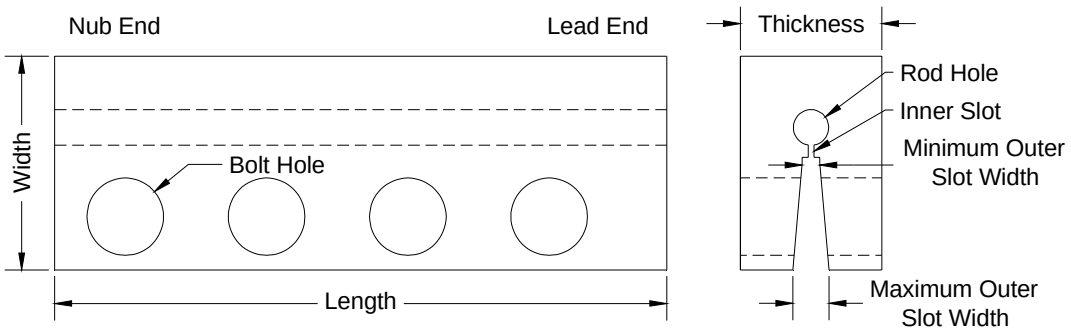

Fig. 3.1 – Unibody clamp anchor geometry

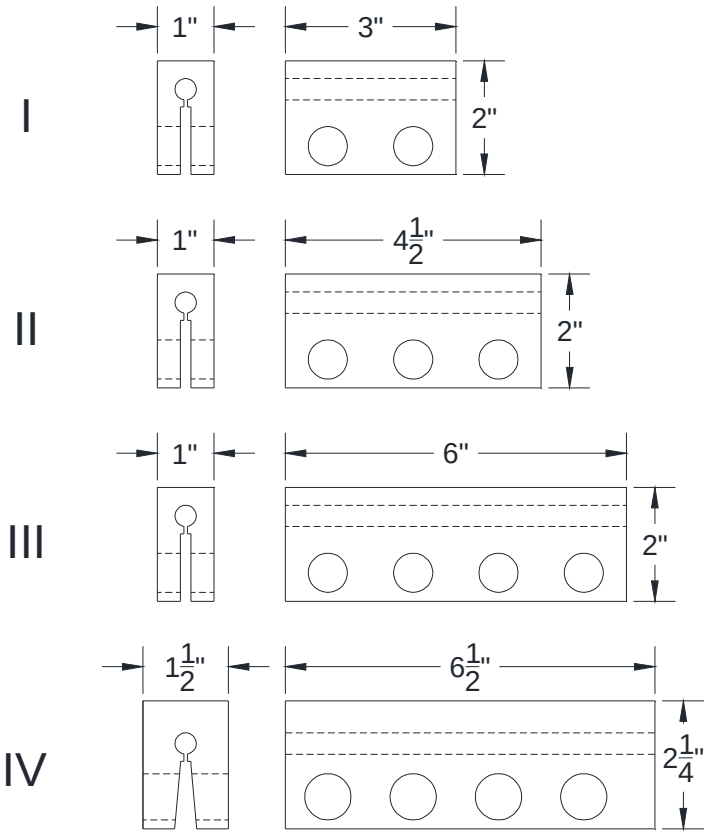

Fig. 3.2 – Anchor size comparison across generations (1” = 25 mm)

Fig. 3.3 – End view of clamped generation IV anchor

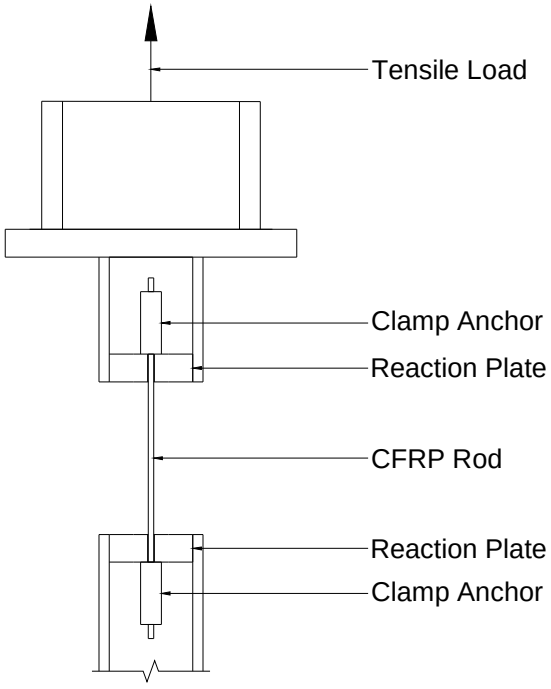

Fig. 3.4 – Test setup

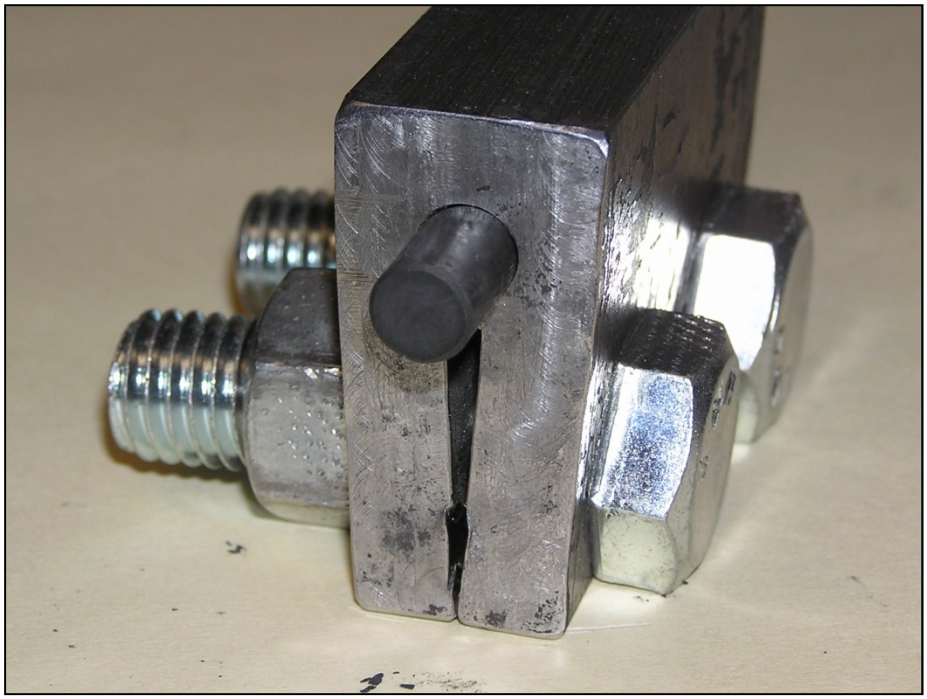

Fig. 3.5 – Generation I anchor

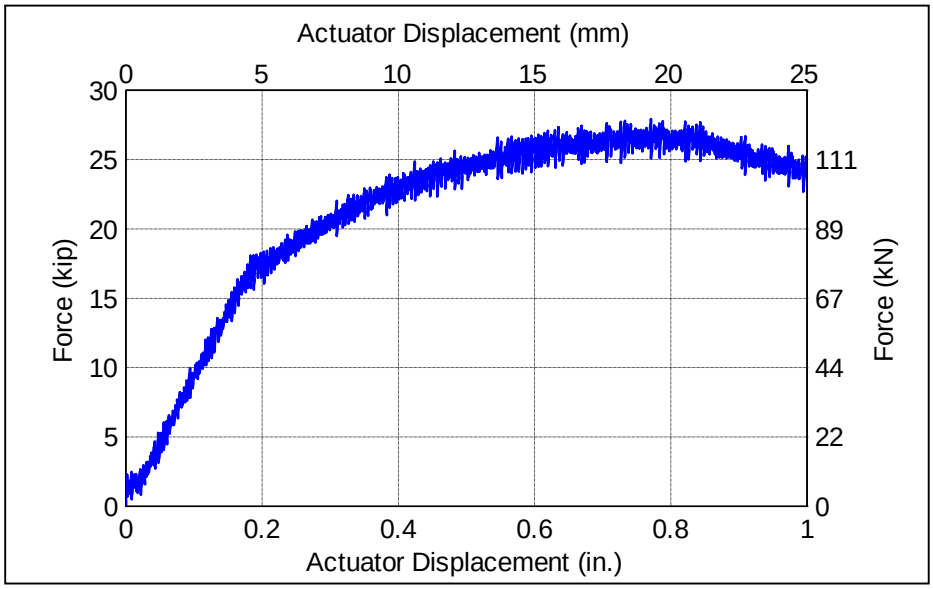

Fig. 3.6 – Generation I anchor applied force vs. actuator displacement

Fig. 3.7 – Damage caused to CFRP rod from slip of generation I anchor

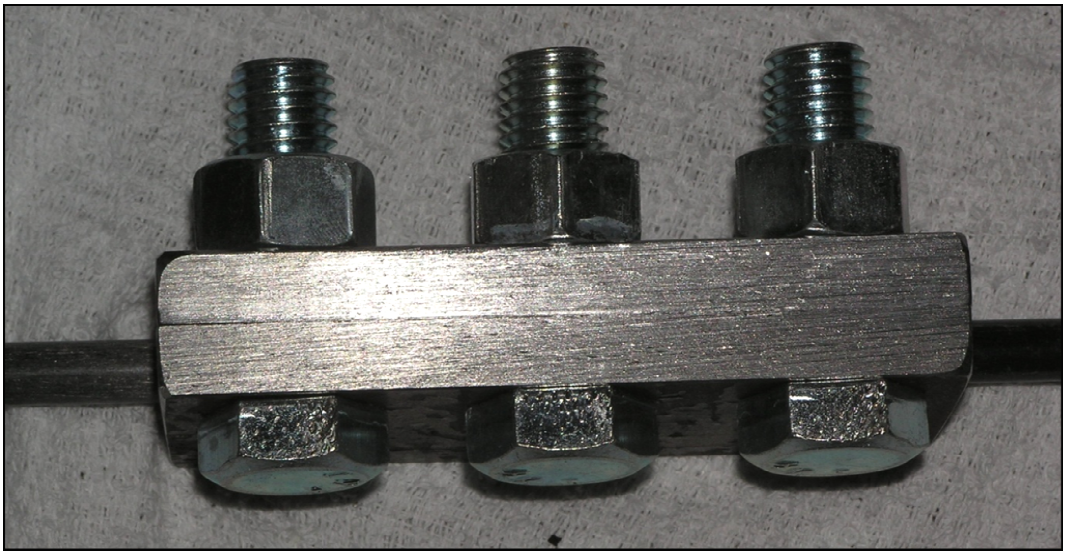

Fig. 3.8 – Generation II anchor

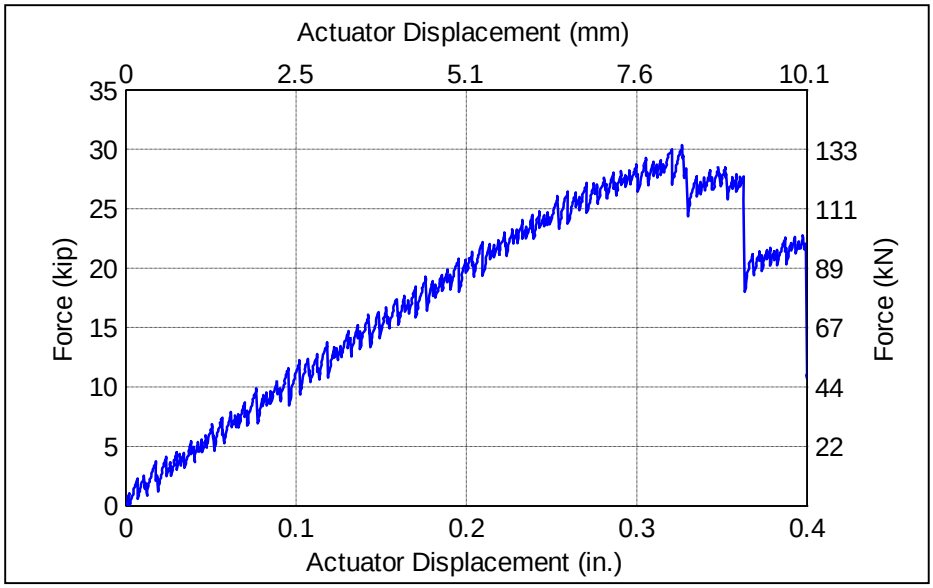

Fig. 3.9 – Generation II anchor applied force vs. actuator displacement

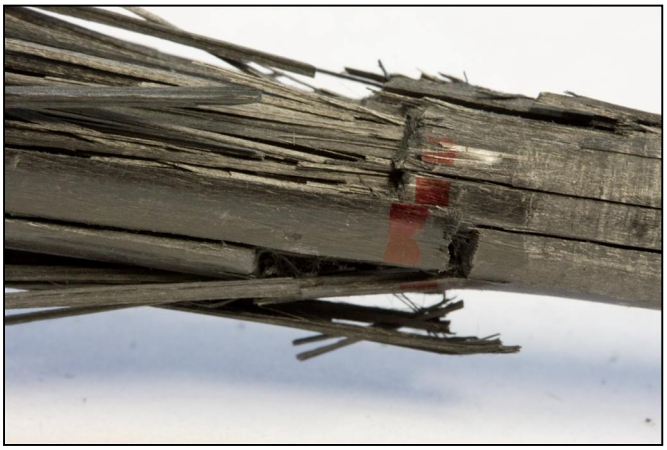

Fig. 3.10 – Ruptured CFRP rod located at lead edge of generation II anchor

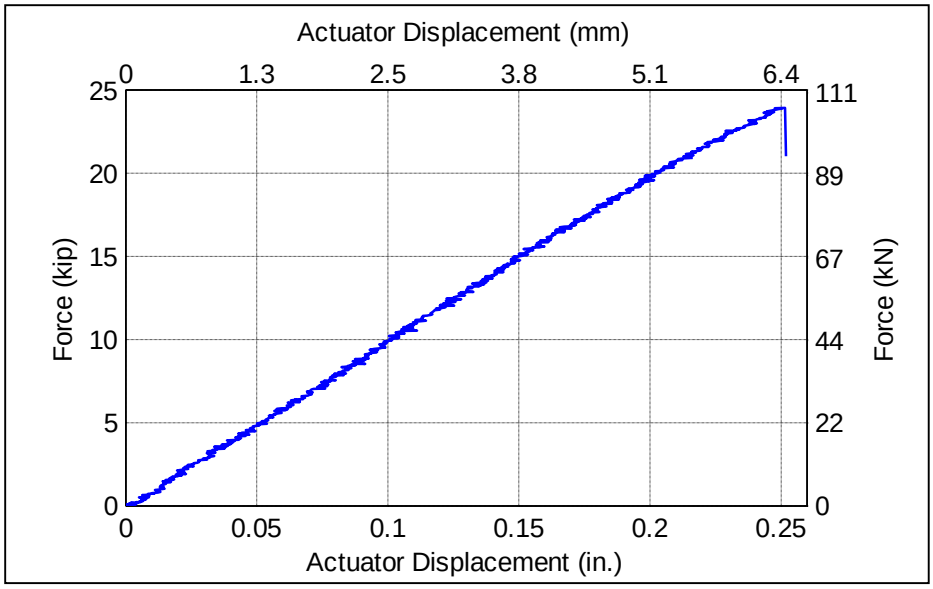

Fig. 3.11 – Generation III anchor applied force vs. actuator displacement

Fig. 3.12 – Failed CFRP rod from generation III anchor

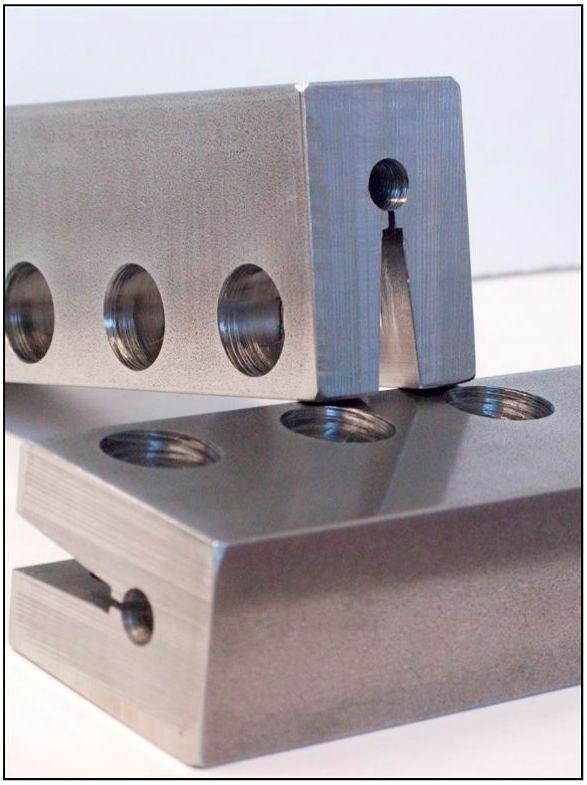

Fig. 3.13 – Unclamped generation IV anchors

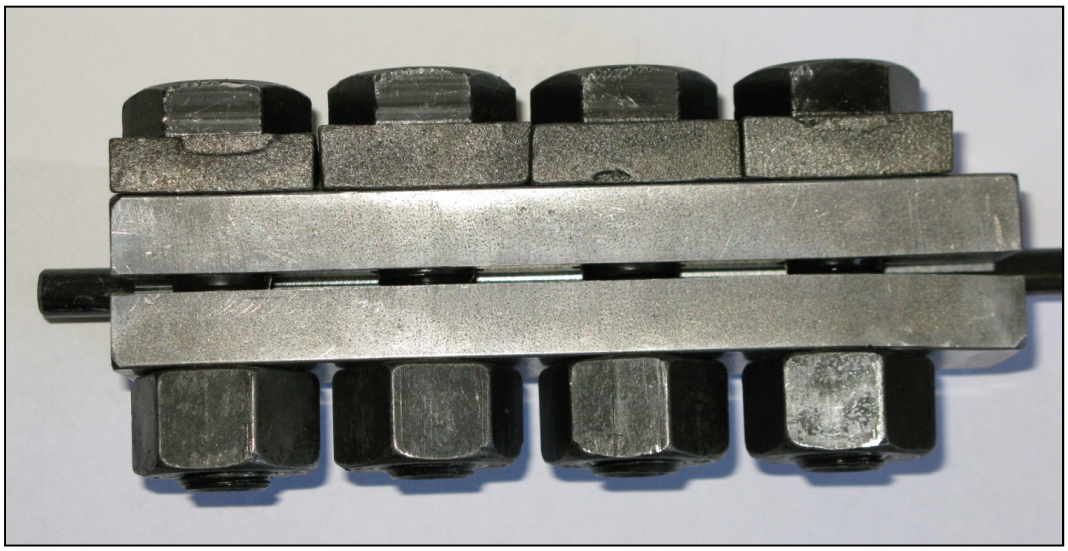

Fig. 3.14 – Clamped generation IV anchor showing increased width of outer slot from left to right

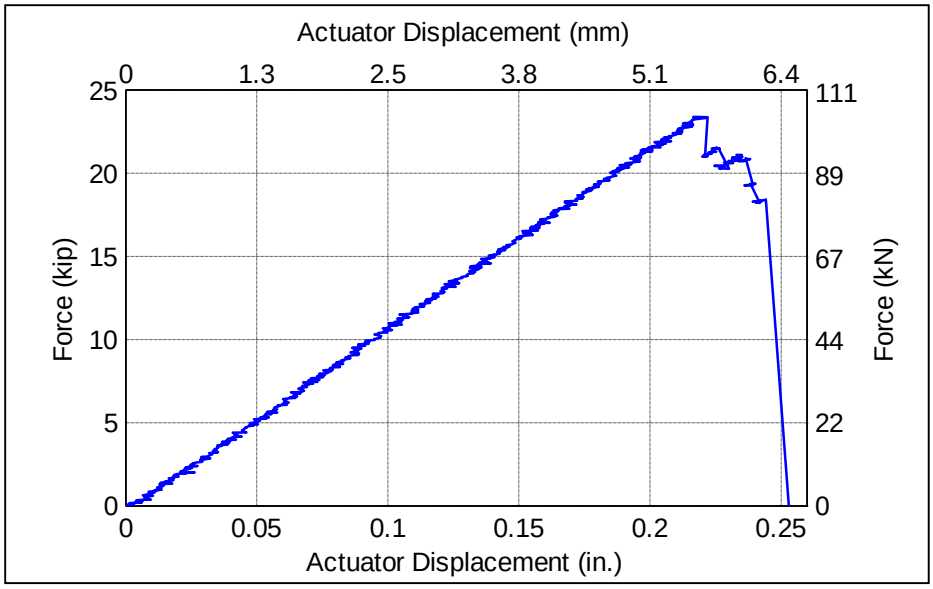

Fig. 3.15 – Generation IV anchor applied force vs. actuator displacement

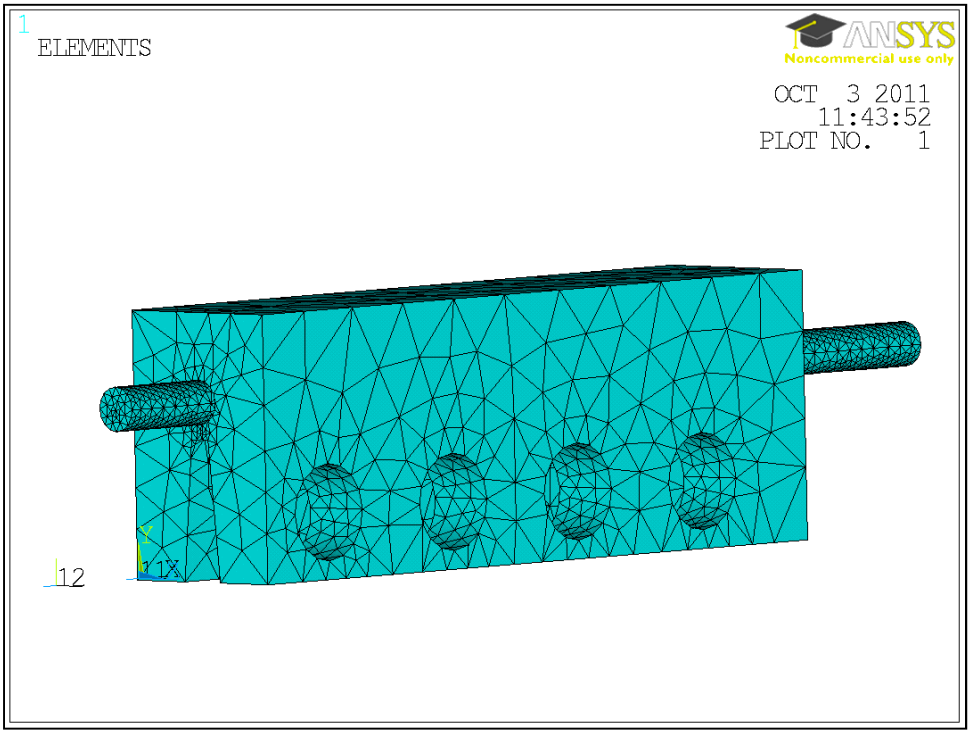

Fig. 3.16 – Generation IV ANSYS geometry and finite element mesh

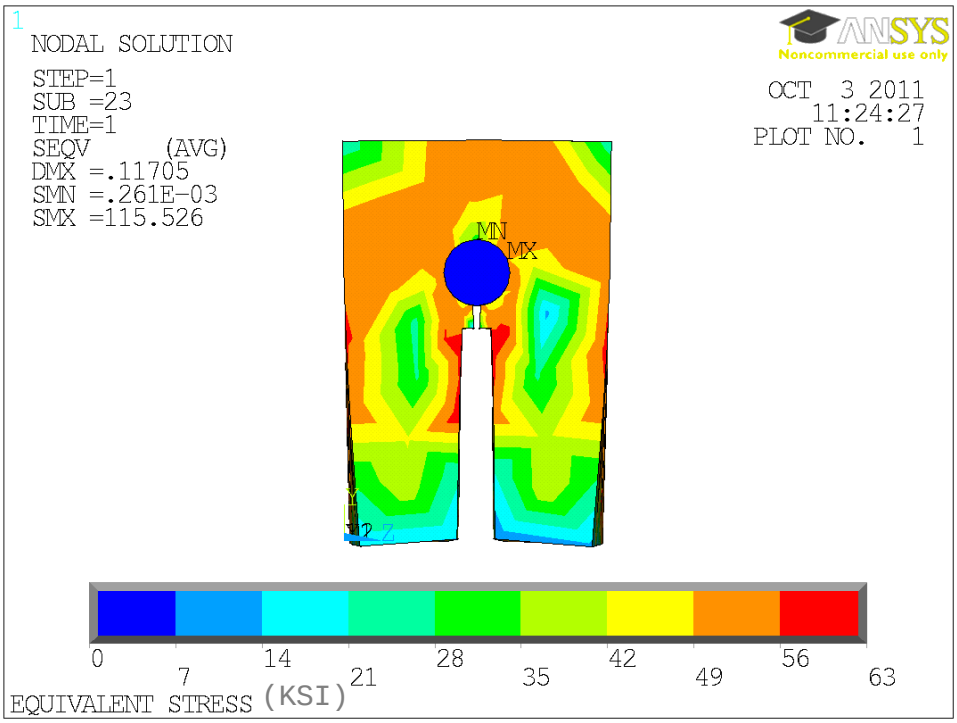

Fig. 3.17 – Equivalent stress plot for generation IV (nub end view)

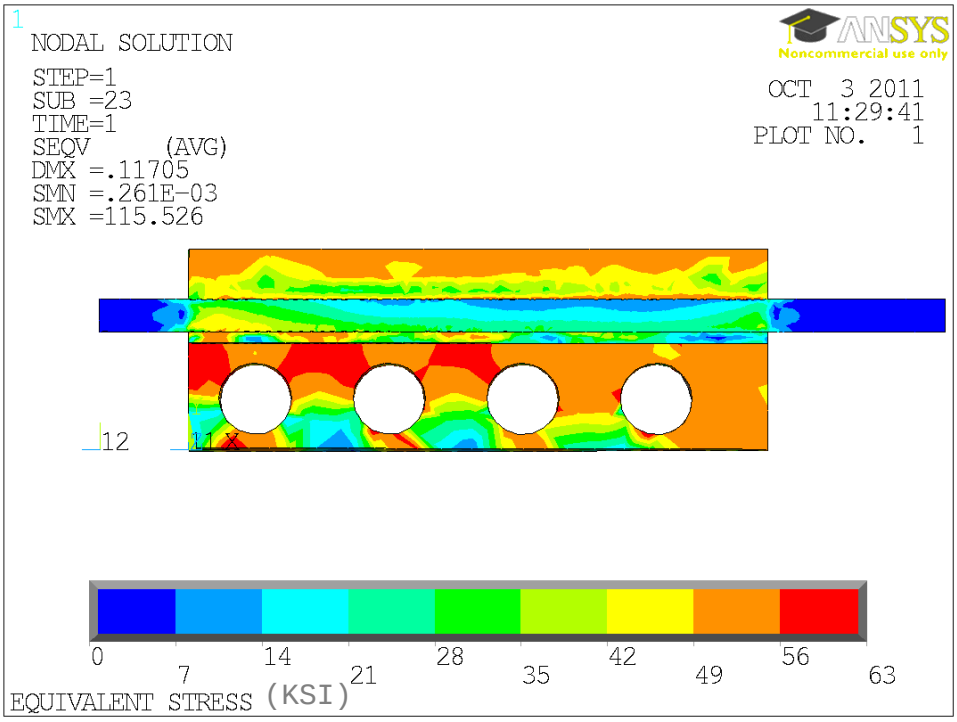

Fig. 3.18 – Equivalent stress plot for generation IV (cross section view)

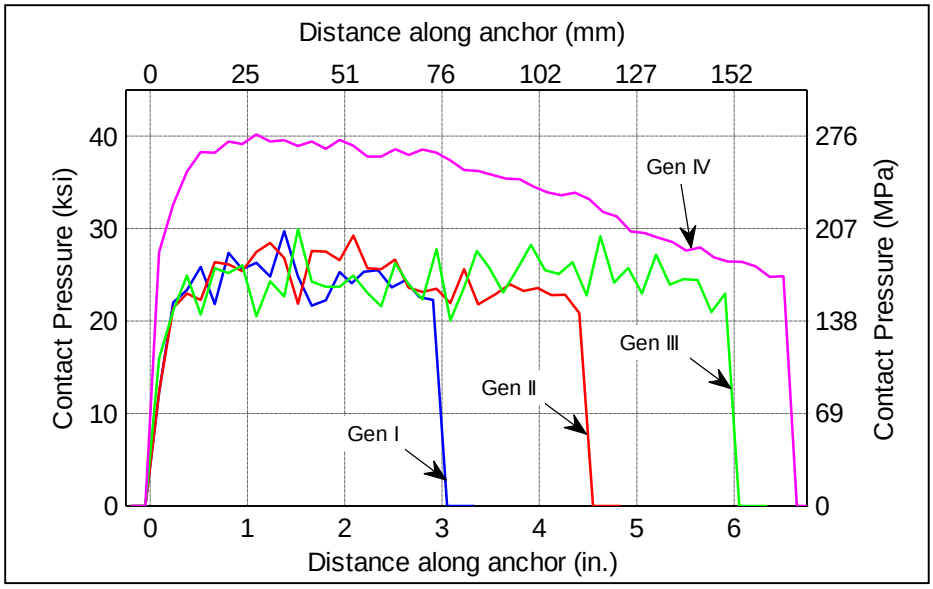

Fig. 3.19 – Change in contact pressure along anchor for generations I-IV (left = nub end and right = lead end)

CHAPTER 4

REPAIR OF SHORT REINFORCED CONCRETE BEAMS USING CFRP POST-TENSIONED RODS

Clayton A. Burningham, Chris P. Pantelides, and Lawrence D. Reaveley

Clayton A. Burningham is a PhD candidate in the department of Civil and Environmental Engineering at the University of Utah. He received his bachelor's and MS degrees from the University of Utah. His research interests include repair of reinforced and prestressed concrete structures and post-tensioning CFRP materials.

ACI member **Chris P. Pantelides** is a Professor and Associate Chair of Civil and Environmental Engineering at the University of Utah. He received his bachelor's degree from the American University of Beirut and his MS and PhD from the University of Missouri-Rolla. His research interests include the seismic design, evaluation, and rehabilitation of reinforced concrete buildings and bridges.

Lawrence D. Reaveley is a Professor and former Department Chair of Civil and Environmental Engineering at the University of Utah. He received his bachelor's and MS degrees from the University of Utah and his PhD from the University of New Mexico. His research interests include structural dynamics with an emphasis on earthquake engineering, vibration problems, and seismic rehabilitation.

(To be submitted for publication)

4.1 Abstract

This paper presents research on the repair of shear damage in reinforced concrete beams using clamp anchors and a mechanical stressing device to post-tension external, unbonded carbon fiber reinforced polymer (CFRP) rods. Specimens in this research were designed to simulate concrete bridge girders with diagonal cracks. Experimental data and a theoretical analysis considering the external CFRP tendons are provided. Based on crack width observations and increases in ultimate capacity, the CFRP repair system was found to be a successful method of repairing reinforced concrete beams with reduced shear capacity due to cracking.

Keywords: CFRP, post-tensioning, repair, retrofit, shear damage, reinforced concrete

4.2 Introduction

Recent attention has been given to the aging transportation infrastructure in the Unites States because of the need to repair or strengthen many existing bridges. Reinforced or prestressed concrete bridge girders can be of particular concern due to damage consisting of diagonal shear cracks that reduce concrete shear capacity and cause internal steel reinforcement to become susceptible to corrosion. Inadequate shear reinforcement or corroded steel reinforcement results in additional shear capacity reduction, increasing the risk of a brittle shear failure. It is imperative that bridges exhibiting symptoms of shear damage and corrosion to shear reinforcement be repaired, strengthened, or replaced.

The repair, rather than the replacement, of damaged reinforced concrete bridge girders is the preferred option because repair is generally less costly and results in a smaller amount of lost time than complete replacement. A possible method of repairing

shear cracks is external post-tensioning, which can close cracks, arrest further crack development, improve concrete shear capacity and friction through aggregate interlock, and increase shear friction within the concrete. However, traditional external post-tensioning has been accomplished with high strength steel tendons which are still susceptible to corrosion and subsequent loss of strength.

On the other hand, fiber reinforced polymer (FRP) materials are corrosion resistant and have a high specific strength. Many of the disadvantages of steel tendons can be overcome with FRP tendons in post-tensioning applications. Previous research has shown that FRP tendons can be used in new construction (Abdel Aziz et al. 2005; El-Hacha and Elbadry 2006; Täljsten and Nordin 2007). Limited research has been conducted using external post-tensioned FRP tendons for the repair of shear damage (Ng 2005; Ng and Soudki 2010). As a result, further investigation is required to determine the suitability of external post-tensioned FRP tendons for the repair of shear cracking and increase of shear capacity in short beams.

One reason for the lack of research involving external post-tensioned FRP tendons is the difficulty in developing an anchor for use with unbonded post-tensioned FRP tendons. Research conducted at the University of Utah has resulted in a clamp anchor and mechanical stressing device for post-tensioning carbon FRP (CFRP) rods. The anchor was developed using small scale pull tests on trial CFRP rods; however, further research is needed to determine the suitability of the anchor for use with the stressing device and CFRP rods post-tensioned on actual concrete members.

This paper presents research involving the application of CFRP rods, University of Utah clamp anchors, and a mechanical stressing device as a complete FRP repair

system for concrete beams with shear damage and associated diagonal shear cracking. Field-observed girder end cracking can be seen in Fig. 4.1. Project details for the specimen fabrication, experimental testing, data results, and theoretical analysis are described. Additionally, details pertaining to the FRP composite system and its application are provided. Finally, conclusions and recommendations regarding the repair system are presented.

4.3 Research Significance

Minimal research has focused on external post-tensioned CFRP tendons for the repair of concrete beams with diagonal shear cracking and inadequate shear capacity. The present research implements unibody clamp anchors and a mechanical stressing device for the repair of reinforced concrete beams with post-tensioned CFRP rods. Additionally, the paper explores the applicability of existing equations for the prediction of the ultimate shear strength of a concrete beam with post-tensioned CFRP tendons. The CFRP anchors and repair system used in this research have the potential to influence industrial acceptance of CFRP post-tensioning systems.

4.4 Experimental Investigation

4.4.1 Specimen Fabrication

Three scaled reinforced concrete (RC) beam specimens were designed and fabricated for this project. The three beams (B12, RB8 and RST8 with “R” indicating a repaired specimen) were constructed at the University of Utah Structures Laboratory and measured 10 in. (254 mm) wide x 24 in. (610 mm) tall x 9 ft (2.74 m) long. The beams had similar longitudinal steel reinforcement arrangements, but differing shear stirrup spacing—the flexural reinforcement in all three specimens consisted of six #5 (ø 16 mm)

bars. Two stirrup spacings were used—8 in. (203 mm) on center for specimens RB8 and RST8, and 12 in. (305 mm) for specimen B12. The 8 in. (203 mm) spacing simulated an appropriate design based on ACI 318-08 beam shear requirements; the 12 in. (305 mm) spacing simulated an inadequate design or corrosion of properly designed shear reinforcement (ACI Committee 318 2008). The stirrups were constructed with #3 (ø 10 mm) bars. Additionally, specimen RST8 had horizontal crack control steel consisting of #3 (ø 10 mm) bars with a vertical spacing of 8 in. (203 mm) along both beam faces. Figure 4.2 shows the reinforcement layout for specimen RB8, and Table 4.1 provides geometric and reinforcement properties for the three specimens.

4.4.2 Experimental Design

All testing was carried out at the University of Utah Structures Laboratory. Diagonal shear cracks were induced using a four point loading system to simulate field observed girder end damage. A hydraulic actuator with a 500 kip (2220 kN) inline load cell and a steel spreader beam were used to apply a two point load spaced 2 ft-6 in. (762 mm) apart at the top of the specimens. Additionally, the specimens were tested with an unbraced length of 7 ft-6 in. (2.29 m). This configuration produced a shear span to depth (a/d) ratio of 1.40, indicating that the beams are short beams controlled by either shear-tension or shear-compression failure. A diagram of the test setup is shown in Fig. 4.3.

4.4.3 Material Properties

All steel reinforcing bars used in the fabrication of the specimens had a nominal tensile strength of 60 ksi (414 MPa), and the beams were constructed in a single concrete batching operation. The compressive strength of the concrete used in the construction of the specimens was 8.6 ksi (59 MPa) at 28 days and 9.3 ksi (64 MPa) at the time of

specimen testing. Additionally, the CFRP rods used in this research had the following manufacturer specified properties: rod diameter = 3/8 in. (9.53 mm), tensile strength = 27.5 kip (122.3 kN), tensile modulus = 22,500 ksi (155 GPa), and elongation at break = 1.1%.

4.4.4 Testing Methods

Specimen testing consisted of three phases: damage, repair, and failure. First, the initial damage loading created diagonal shear cracks in specimens B12, RB8 and RST8, simulating field-observed girder end cracking. Next, the repair system of unibody clamp anchors and post-tensioned CFRP rods was applied to specimens RB8 and RST8. Finally, specimens B12, RB8, and RST8 were loaded to failure.

Initial damage loading was used to induce diagonal cracks and simulate field-observed damage. The loading was displacement controlled to induce similar damage to all three specimens and avoid sudden failure and subsequent loss of the specimens. Displacement half-cycles were applied in increments of 0.0625 in. (1.59 mm), with the amplitude of each successive half-cycle increasing by 0.0625 in. (1.59 mm). In addition, the rate of displacement was held constant at 0.0625 in./min (1.59 mm/min) throughout the test. A typical crack pattern showing the diagonal cracks near the beam ends can be seen in Fig. 4.4. All specimens were subjected to the abovementioned loading protocol, with termination of the loading dependent upon visible cracking, deflected shape data, and force versus actuator displacement data. Testing procedures were paused after each half-cycle to aid in crack inspection, marking, and documentation. The maximum deflection of specimens RB8 and RST8 during the initial damage loading was approximately 70% and 39% greater than that of specimen B12, respectively. This

increase in deflection ensured significant cracking occurred in the specimens to be repaired. The maximum observed crack widths after the initial damage loading for specimens B12, RB8, and RST8 were 0.020 in. (0.5 mm), 0.040 in. (1.0 mm), and 0.035 in. (0.9 mm), respectively.

After the initial loading to create diagonal cracks simulating girder end cracking, specimens RB8 and RST8 were repaired with a system of clamp anchors, a mechanical stressing device, and external post-tensioned CFRP rods. Both specimens were repaired with four rods, two on each side of the beam. The top and bottom level of tendons were at a depth of 11 in. (279 mm) and 19 in. (483 mm) from the top compression fiber of the beam, respectively. Additionally, the CFRP rods were post-tensioned to a strain of approximately 0.485%, producing a post-tensioning force of 12 kips (53.4 kN) in each rod. This level of initial post-tensioning force was selected based on the recommended range of 40 to 65% of ultimate strength given in ACI 440.4R-04 for FRP tendons (ACI Committee 440 2004).

Figures 4.5 and 4.6 show the dual layer tendon stressing mechanism used on specimens RB8 and RST8. The stressing device consists of a slotted square HSS section running perpendicular to the beam length at the live stressing end of the beam. The tendons pass through the slots, and the unibody clamp anchors make contact with the back side of the tube. Four sleeve nuts (two on top and two on bottom) are positioned on the HSS section perpendicular to the HSS section and parallel with the beam. Tendon stressing occurs when 1.0 in. (25 mm) diameter bolts are screwed into the sleeve nuts; the bolts react against the beam end, moving the HSS section back to stress the tendons.

Tightening the stressing bolts in an alternating star pattern ensures the tendons are stressed with controlled increments of tightening.

After repairing specimens RB8 and RST8 with external post-tensioned CFRP rods, all three specimens were loaded to failure monotonically at a rate of 0.0625 in./min (1.59 mm/min). Termination of the loading depended on failure of the specimen—defined as a 20% decrease in maximum applied load or tensile failure of the external CFRP rods, whichever occurred first.

4.5 Experimental Results

4.5.1 Data Collection Methods

The specimens were instrumented with strain gauges and linear variable differential transformers (LVDTs), with data collection occurring at a rate of two points per second. All LVDT readings were measured within 0.001 in. (0.025 mm).

4.5.2 Instrumentation

Three LVDTs—one located 34.1” (0.87 m) from either beam end and one at midspan—were used on the bottom of the beam to measure the deflected shape under load. Compressive strains in the concrete on the top face of the beam were measured by strain gauges placed at 33.5 in. (0.85 m) from each beam end and at midspan. Strain gauges were also placed on the internal longitudinal steel reinforcement and stirrups of all specimens and on the CFRP rods at midspan for specimens RB8 and RST8.

4.5.3 Specimen Data Analysis

Specimen B12 (control) failed due to concrete crushing between interior loading points at the beam top compression fiber. Likewise, specimen RB8 (repaired) failed at

later stages due to concrete crushing failure between loading points at the beam top compression fiber after rupture of the lower and upper level external CFRP rods. Similar to specimen RB8 (repaired), specimen RST8 (repaired) failed due to concrete crushing failure between loading points after the lower external CFRP rods ruptured; however, the upper level CFRP rods remained intact and never failed. Specimens B12, RB8, and RST8 at failure can be seen in Figs. 4.7-4.9, respectively.

The compressive strain in the concrete was highest at midspan. Fig. 4.10 shows the change in compressive strain at midspan with the change in applied load. As seen in Fig. 4.10, all three specimens had compressive strains approaching 0.25%, indicating likely compressive failure from concrete crushing. These strains are consistent with the concrete crushing observed in specimens B12, RB8, and RST8 and seen in Figs. 4.7-4.9, respectively.

The strains in the CFRP rods for specimens RB8 and RST8 were also monitored during testing. Fig. 4.11 shows the strain in the bottom CFRP rods of specimens RB8 and RST8 during loading to failure. Additionally, Fig. 4.12 shows the strain in the top CFRP rods of specimen RB8 during loading to failure. Initially, after the repair phase and application of the post-tensioning system, the strain in the rods was 0.485%. At the time of rupture, the average strain in the lower CFRP rods for specimens RB8 and RST8 increased to a maximum—0.854% and 0.877%, respectively, as shown in Fig. 4.11. Additionally, for specimen RB8, the average strain in the upper CFRP tendons at the time of rupture was 0.789%. Since the ultimate strain of the rods is 1.1%, stress concentrations at a point other than midspan, where the strain gauges were installed, caused rupture of the rods. One factor that may cause a local stress concentration is the geometric effect of

large deflections. As large deflections occur, the beam ends rotate while the tendon maintains a level position. This rotation at the beam ends causes flexure to be introduced into the CFRP rods rather than just pure tension, possibly leading to premature tendon failure from the resulting stress concentrations.

An increase in the observed ultimate capacity compared to the control specimen indicates that the CFRP repair system was successful. The ultimate load for specimen B12 (control), RB8 (repaired) and RST8 (repaired) was 301 kips (1339 kN), 381 kips (1695 kN), and 375 kips (1668 kN), respectively. Additionally, the applied load versus midspan deflection during initial damage loading and loading to failure is shown in Figs. 4.13-4.15. When compared to the control specimen, the ultimate loads correspond to an increase in capacity of approximately 27% for specimen RB8 and 25% for specimen RST8—simply from the CFRP repair system. It is also of note that Fig. 4.14 clearly shows the drop in applied load when the lower and upper CFRP rods ruptured for specimen RB8 at approximately 0.96 in. (24.4 mm) and 1.54 in. (39.1 mm) midspan deflection, respectively. Similarly, Fig. 4.15 shows the drop in applied load when the lower level CFRP rods ruptured for specimen RST8 at approximately 0.95 in. (24.1 mm) midspan deflection.

From Fig. 4.16, it can be seen that failure of the bottom layer CFRP rods for specimens RB8 and RST8 occurred at deflections over eight times greater than L/800 (0.11 in. or 2.86 mm), the maximum allowable design deflection for concrete bridge construction (AASHTO 2009). Therefore, although failure of the lower CFRP rods was brittle, this failure occurred at a deflection much greater than anticipated deflections from service loads. It can also be seen from Fig. 4.16 that after failure of the upper and lower

CFRP rods, specimen RB8 exhibited a residual strength of approximately 317 kips (1410 kN), and after failure of the upper CFRP rods for specimen RST8, a residual strength of approximately 293 kip (1303 kN) was observed. This is evidence that even though the CFRP rods ruptured in a brittle failure mechanism, complete catastrophic failure of the repaired beams did not occur because of the ductility of the base system.

4.6 Analytical Investigation

Much of the previous research has been devoted to strut-and-tie models as a method of design for short or deep beams. The following section will assess the applicability of strut-and-tie models for the high strength concrete beams in the present research. Additionally, equations accounting for beam action and arch action for the prediction of shear strength will be evaluated to determine their suitability for use in relation to the specimens tested in this research.

4.6.1 Strut-And-Tie Model

A strut-and-tie model was developed for the control specimen and the two repaired specimens. The model for specimen B12 (control) can be seen in Fig. 4.17 where the dashed lines represent compression struts and the solid lines represent tension ties. This model predicts an ultimate capacity for specimen B12 (control) of 180 kip (801 kN). Comparing this theoretical value to the actual ultimate load of 301 kip (1339 kN) yields a ratio of actual to theoretical ultimate load of 1.7.

A similar model was developed for repaired specimens RB8 and RST8 by accounting for the two levels of external post-tensioned CFRP rods. The same strut-and-tie model was used for both RB8 and RST8 as they had identical stirrup spacing, internal longitudinal steel reinforcement, and external CFRP rod placement—with the only

difference being the inclusion of minor crack control steel in specimen RST8. For both specimen RB8 and RST8, the experimental average strains at midspan in the internal longitudinal steel and external CFRP rods were used in the development of the strut-and-tie forces.

Figure 4.18 illustrates this model which predicts an ultimate load of 204 kip (907 kN) and 206 kip (916 kN) for specimens RB8 and RST8, respectively. Compared to the respective actual loads of 381 kips (1695 kN) and 375 kips (1668 kN) for specimens RB8 and RST8, ratios of actual to theoretical ultimate load of 1.9 and 1.8 result, respectively. A summary of the experimental and theoretical loads produced by the strut-and-tie method can be seen in Table 4.2.

Currently, the strut-and-tie method is allowed for deep beam design by ACI 318-08, and the control specimen B12 functions as an example of the style of beam that may be designed according to this provision (ACI Committee 318 2008). Furthermore, comparing the ratios of actual to theoretical ultimate loads shows that the strut-and-tie model predictions for specimens RB8 (repaired) and RST8 (repaired) are more conservative than that of specimen B12 (control). Therefore, since the strut-and-tie model for the repaired specimens produces ultimate load predictions that are more conservative than that of the control specimen—which is currently able to be designed with a strut-and-tie model under ACI 318-08 provisions—strut-and-tie models may be an appropriate method for the design of beams for which the repair system of external post-tensioned CFRP rods presented in this research is to be implemented. However, it should be noted that ACI 318-08 limits the use of strut-and-tie models for design to members with a concrete compressive strength no greater than 6000 psi (41.4 MPa). Since the concrete

strength of the specimens tested in this research was 9300 psi (64 MPa), further research is needed to determine whether or not strut-and-tie models are appropriate for the design of all short or deep beams made from high strength concrete, and in particular, high strength concrete beams rehabilitated with external post-tensioned CFRP tendons.

4.6.2 Equations Predicting Shear Capacity

In addition to investigating the use of a strut-and-tie model for design, several equations from the literature were examined for the prediction of ultimate shear capacity. One historic equation for the prediction of mean ultimate shear stress was developed by Zsutty (Zsutty 1968; Zsutty 1971). Statistically developed from test data, the equation accounted for the contribution of the concrete to shear resistance, but did not account for internal steel stirrups. Seeking to improve upon the concepts pioneered by Zsutty, Bažant and Kim (1984) developed a mean ultimate shear stress prediction equation accounting for beam and arch action based on mechanics. Additionally, Bažant and Kim developed an empirically based function to account for the size effect in reinforced concrete.

Russo and Puleri (1997) further developed the equation developed by Bažant and Kim to include the contribution of steel shear reinforcement to shear resistance, as follows:

$$v_u = 0.83\xi\chi\sqrt[3]{\rho} + 1.67\frac{\sqrt{f'_c}}{\chi}\rho_v f_{yv} \tag{4.1}$$

where v_u is the mean ultimate shear stress in MPa; ξ is the function accounting for size effect; ρ is the longitudinal steel reinforcement ratio; f'_c is the concrete compressive strength in MPa; ρ_v is the stirrup reinforcement ratio; and f_{yv} is the yield strength of the stirrup reinforcement in MPa. The variable χ is given as:

$$\chi = \sqrt{f'_c} + 250\sqrt{\rho\left(\frac{d}{a}\right)^5} \tag{4.2}$$

where f'_c is in MPa; d is the effective depth of the section; and a is the shear span. Additionally, the size effect function developed by Bažant and Kim in Eq (4.1) is given as:

$$\xi = \frac{1}{\sqrt{1+\frac{d}{25d_a}}} \tag{4.3}$$

where d_a is the maximum aggregate size (Bažant and Kim 1984). It should be noted that the equation developed by Russo and Puleri accounts for arch action, beam action, and the effect of stirrups, but does not account for external post tensioning. Ng (2005) tried to overcome this limitation by suggesting the following equation for ultimate shear capacity based on the work of Bažant and Kim:

$$V_u = \left(0.83\xi\chi\sqrt[3]{\rho} + 1.67\frac{\sqrt{f'_c}}{\chi}\rho_v f_{yv}\right)bd + T_f\frac{dz}{dx} \tag{4.4}$$

where V_u is the ultimate shear capacity; b is the width of the beam; T_f is the force in the external post-tensioning at ultimate and $\frac{dz}{dx}$ is the rate of change in the internal moment arm. According to Ng (2005), the additional term in Eq. (4.4) accounts for an increase in shear capacity of a beam with external, unbonded prestressing.

Additionally, Ng argues that since Eq. (4.1) was originally standardized based on test data for normally reinforced concrete specimens, there are some limitations when extending the equation to beams with prestressing reinforcement. Ng suggests that in the absence of additional research to restandardize Eq. (4.1) for beams with prestressing

reinforcement, an equivalent shear span, a_{eq}, may be used in conjunction with Eq. (4.4) to produce ultimate shear strength predictions similar to those traditionally obtained for normally reinforced concrete beams. According to Ng (2005), a conservative value for the equivalent shear span may be found from

$$a_{eq} = \frac{M_{non-ps\_u}}{M_{ps\_u}} a \tag{4.5}$$

where M_{non-ps_u} is the ultimate moment capacity of a similar beam without prestressing reinforcement, and M_{ps_u} is the ultimate capacity of the beam with external, unbonded prestressing.

In addition to the equivalent shear span, Ng proposes that the additional term in Eq. (4.4) accounts for the increase in ultimate shear strength caused by the increase in arch action from external, unbonded prestressing. Furthermore, the rate of change of the internal moment arm is given by

$$\frac{dz}{dx} = \frac{r \times jd}{{a_{eq}}^r} x^{r-1} \tag{4.6}$$

where $r = k\left(\frac{d}{a_{eq}}\right)^{n1} \rho^{n2} \leq 1$, with $k = 0.6$, $n1 = 1.4$, and $n2 = -0.2$ for beams with stirrups and jd is the moment arm at the shear span distance from the support (Ng 2005).

The evaluation of Eq. (4.3) for the specimens in this research with an effective depth of 21.4 in. (544 mm) and a maximum aggregate size of 0.75 in (19 mm) yields a size effect factor equal to 0.61. It is the authors' opinion that this factor results in overly conservative estimates of the ultimate shear strength of specimens B12, RB8, and RST8. Furthermore, visual inspection during concrete cylinder tests and the testing of the three

specimens in this research showed concrete failure progressing through the aggregate—not around the aggregate; this observation is attributed to the high strength concrete used to construct the beams. Furthermore, the extremely conservative results from the use of Eq. (4.3) for the specimens in this research suggest that Eq. (4.3) may need to be re-calibrated for use with high-strength concrete specimens. In the absence of further testing with high strength concrete, the size effect factor ξ of Eq. (4.3) was assumed to be equal to one.

For the specimens in this research with $\xi = 1$, a shear span of 30 in. (762 mm), a moment arm at a distance of the shear span from the support of 17.6 in (447 mm), and using the experimental strains measured in the CFRP rods, Eq. (4.1) can be used for specimen B12 (control) since there is no prestressing involved, and Eq. (4.4) for specimens RB8 (repaired) and RST8 (repaired) to predict specimen ultimate shear capacity. The predicted capacities of B12 (control), RB8 (repaired), and RST8 (repaired) were found to be 226 kip (1005 kN), 395 kip (1757 kN), and 400 kip (1779 kN), respectively. Comparing these theoretical ultimate loads to the experimental ultimate loads results in respective ratios of 1.33, 0.97, and 0.94 for specimens B12 (control), RB8 (repaired), and RST8 (repaired). A summary of the experimental and theoretical loads produced by Eqns. (4.1), (4.3), and (4.4) can be seen in Table 4.3.

The ratios of theoretical to ultimate loads for specimens RB8 (repaired) and RST8 (repaired) suggest that Eq. (4.4) may be suitable for predicting the ultimate shear strength of beams repaired with the unibody clamp anchors, mechanical stressing device, and CFRP rods implemented in this research. However, since the ratios are less than one, the results are clearly not conservative; subsequently, it is not recommended that Eq. (4.4) be

used for design purposes without, as Ng suggests, further research to properly calibrate Eq. (4.4) for beams with prestressed reinforcement. Additionally, the authors of this paper recommend that the effects of high strength concrete on size effect be further examined to recalibrate Eqns. (4.3) and (4.4).

4.7 Conclusions

The experimental results from this research show that two concrete beams with diagonal cracks (RB8 and RST8) were successfully repaired with unibody clamp anchors, a novel mechanical stressing device, and CFRP rods. Repaired specimens RB8 and RST8 showed a 27% and 25% increase in ultimate strength compared to control specimen B12, respectively. Additionally, rupture of the post-tensioned CFRP rods occurred at deflections eight times larger than the AASHTO maximum allowable deflection, indicating a high level of safety regarding serviceability requirements. Since the unibody clamp anchors, mechanical stressing device, and CFRP rods were successfully implemented for the repair of the specimens in this research, it is recommended that additional research be conducted regarding field application and general use of the system.

A strut-and-tie model was developed for the repaired concrete beams RB8 and RST8; the model was found to produce ratios of experimental to theoretical ultimate load higher than that of control specimen B12, indicating that a strut-and-tie model may be used to design the repair system of clamp anchors and external post-tensioned CFRP rods applied to the specimens in the present research. However, additional research should be conducted to determine the suitability of strut-and-tie models in situations where high strength concrete members are repaired with external post-tensioned CFRP tendons.

A theoretical expression from the literature originally developed for use with reinforced concrete beams was found to predict the ultimate capacity of the repaired specimens within 6%, but was unconservative. It is suggested that further research be conducted to calibrate the equation for use with high strength concrete beams with post-tensioned external CFRP tendons.

It is recommended that the clamp anchors be studied further to determine their suitability as a coupling device for CFRP rods. This will facilitate the use of the CFRP rods for post-tensioning applications with typically longer spans than those of the specimens in this research. Furthermore, the implementation of the repair system in this paper requires 18” (0.46 m) of free space behind the beam; since access is not always available in the field, mechanical anchorage might be attached to the bottom surface, flange bottom, or beam web to allow the beam to be post-tensioned along a portion of the span or the entire span as required.

4.8 Acknowledgements

The authors wish to acknowledge the financial support of the Utah Department of Transportation and the University of Utah, as well as in-kind contributions from Geneva Rock Products, Inc., and Sika, Inc. Additionally, the authors would like to thank Brandon Besser, Mark Bryant, Megan Crump, Jack Furbush, Mike Gibbons, Ruifen Liu, Yasuteru Okahashi, Brett Raddon, Eric Smith, Max Wood, and Arthur Yeomans for their assistance in specimen fabrication and testing.

4.9 Notation

a = shear span

a_{eq} = equivalent shear span

b = beam width

d = depth to longitudinal reinforcement (effective depth)

d_a = maximum aggregate size

f'_c = concrete compressive strength

f_{yv} = yield strength of stirrups

jd = moment arm distance at the shear span length

M_{non-ps_u} = ultimate moment capacity of similar beam without prestressing

M_{ps_u} = ultimate moment capacity of beam with prestressing

T_f = force in external post-tensioning at ultimate

V_u = ultimate shear capacity

v_u = mean ultimate shear stress

ρ = longitudinal steel reinforcement ratio

ρ_v = stirrup reinforcement ratio

4.10 References

Abdel Aziz, M.; Abdel-Sayed, G.; Ghrib, F.; Grace, N.; and Madugula, M., 2005, "Analysis of Concrete Beams Prestressed and Post-Tensioned with Externally Unbonded Carbon Fiber Reinforced Polymer Tendons," *Canadian Journal of Civil Engineering*, V. 31, pp. 1138-1151.

ACI Committee 318, 2008, "Building Code Requirements for Reinforced Concrete (ACI 318-08) and Commentary (ACI 318R-08)," American Concrete Institute, Farmington Hills, MI.

ACI Committee 440, 2004, "Prestressing Concrete Structures with FRP Tendons (ACI 440.4R-04)," American Concrete Institute, Farmington Hills, MI.

AASHTO, 2009, "AASHTO LRFD Bridge Design Specifications (4th Edition)," American Association of State Highway and Transportation Officials, Washington DC.

Bažant, Z. P., and Kim, J. K., 1984, "Size Effect in Shear Failure of Longitudinally Reinforced Beams," *ACI Structural Journal*, V. 81, No. 5, pp. 456-468.

El-Hacha, R., and Elbadry, M., 2006, "Strengthening Concrete Beams With Externally Prestressed Carbon Fiber Composite Cables: Experimental Investigation," *PTI Journal*, V. 4, No. 2, pp. 53-70.

Ng, S., 2005, "Shear Behaviour of RC Beams Externally Prestressed with CFRP Rods," Master's thesis, University of Waterloo, Waterloo, Ontario.

Ng, S., and Soudki, K., 2010, "Shear Behavior of Externally Prestressed Beams with Carbon Fiber-Reinforced Polymer Tendons," *ACI Structural Journal*, V. 108, No. 4, pp. 443-450.

Russo, G., and Puleri, G., 1997, "Stirrup Effectiveness in Reinforced Concrete BEams under Flexure and Shear," *ACI Structural Journal*, V. 94, No. 3, pp. 227-238.

Täljsten, B., and Nordin, H., 2007, "Concrete Beams Strengthened with External Prestressing Using External Tendons and Near-Surface-Mounted Reinforcement," ACI SP-245, pp. 143-164.

Zsutty, T. C., 1968, "Beam Shear Strength Prediction by Analysis of Existing Data," *ACI Journal*, V. 65, No. 11, pp. 943-951.

Zsutty, T. C., 1971, "Shear Strength Prediction by Analysis of Existing Data," *ACI Journal*, V. 68, No. 2, pp. 138-143.

Table 4.1 –Specimen geometry and reinforcement details

Specimen	Width	Height	Length	Shear Reinforcement	Flexure Reinforcement
B12 (control)	10 in. (254 mm)	24 in. (610 mm)	9.0 ft (2.74 m)	#3 (ø 10mm) stirrups at 12 in. (305 mm)	6 - #5 bars (ø 16 mm)
RB8 (repaired)	10 in. (254 mm)	24 in. (610 mm)	9.0 ft (2.74 m)	#3 (ø 10mm) stirrups at 8 in. (203 mm)	6 - #5 bars (ø 16 mm)
RST8 (repaired)	10 in. (254 mm)	24 in. (610 mm)	9.0 ft (2.74 m)	#3 (ø 10mm) stirrups at 8 in. (203 mm)	6 - #5 bars (ø 16 mm)

Table 4.2 – Experimental and strut-and-tie loads at ultimate

Specimen	Experimental Ultimate Load	Theoretical Ultimate Load	Ratio of Experimental to Theoretical Ultimate Load
B12 (control)	301 kip (1339 kN)	180 kip (801 kN)	1.7
RB8 (repaired)	381 kip (1695 kN)	204 kip (907 kN)	1.9
RST8 (repaired)	375 kip (1668 kN)	206 kip (916 kN)	1.8

Table 4.3 – Experimental and theoretical equation predicted loads at ultimate

Specimen	T_f	a_{eq}	Experimental Ultimate Load	Theoretical Ultimate Load	Ratio of Experimental to Theoretical Ultimate Load
B12 (control)	n/a	n/a	301 kip (1339 kN)	226 kip (1005 kN)	1.33
RB8 (repaired)	42.3 kip (188 kN)	22.7 in. (578 mm)	381 kip (1695 kN)	395 kip (1757 kN)	0.97
RST8 (repaired)	43.4 kip (193 kN)	22.6 in. (575 mm)	375 kip (1668 kN)	400 kip (1779 kN)	0.94

Fig. 4.1 – Girder end damage with diagonal cracking

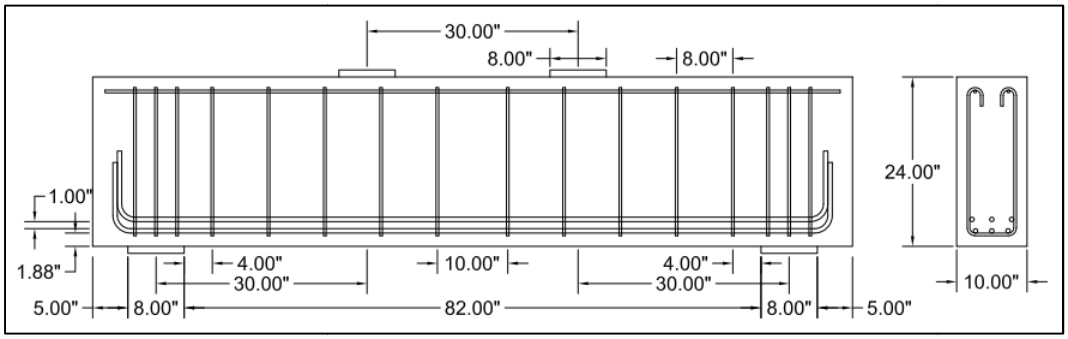

Fig. 4.2 – Reinforcement layout for specimen RB8
(1 in. = 25.4 mm; #3 = ø 10 mm; #5 = ø 16 mm)

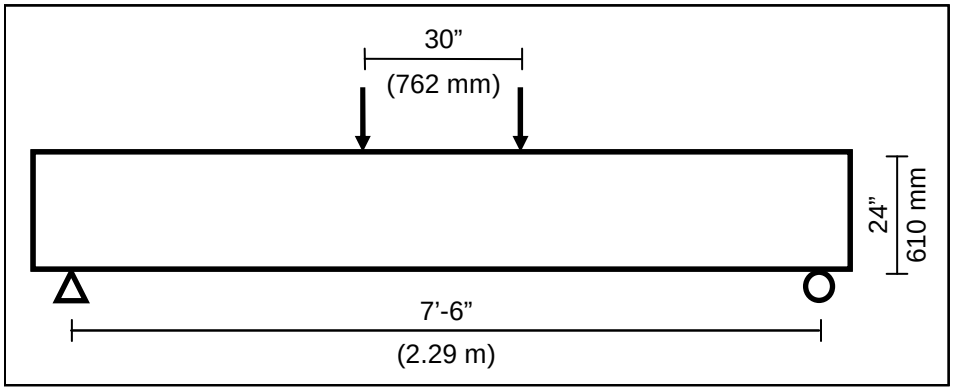

Fig. 4.3 – Test setup

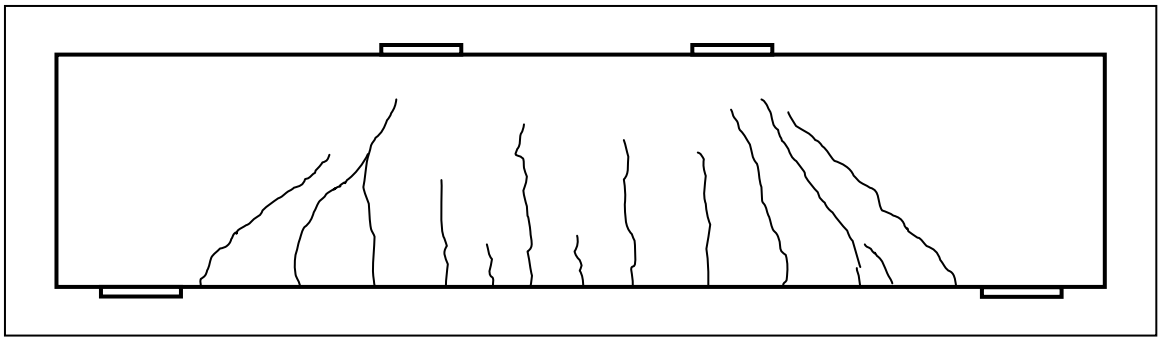

Fig. 4.4 – Typical crack pattern

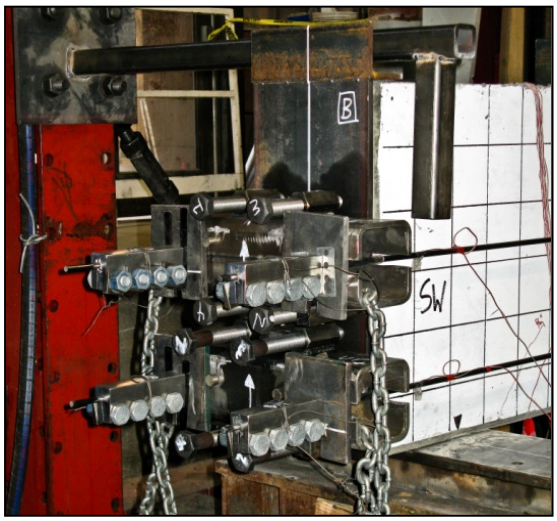

Fig. 4.5 – End view of two level stressing system

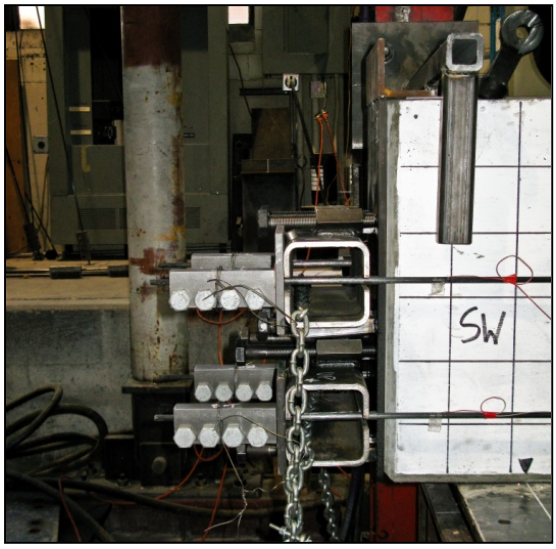

Fig. 4.6 – Side view of two level stressing system

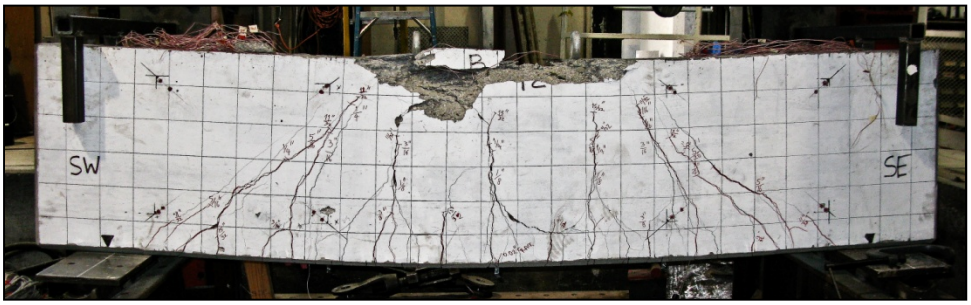

Fig. 4.7 – Failed specimen B12 (control)

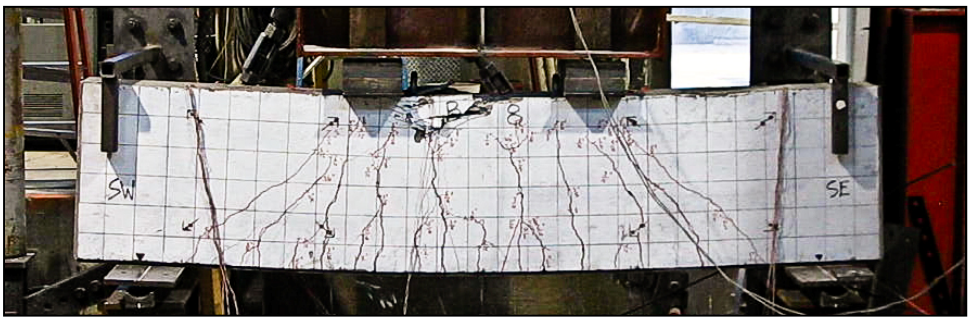

Fig. 4.8 – Failed specimen RB8 (repaired)

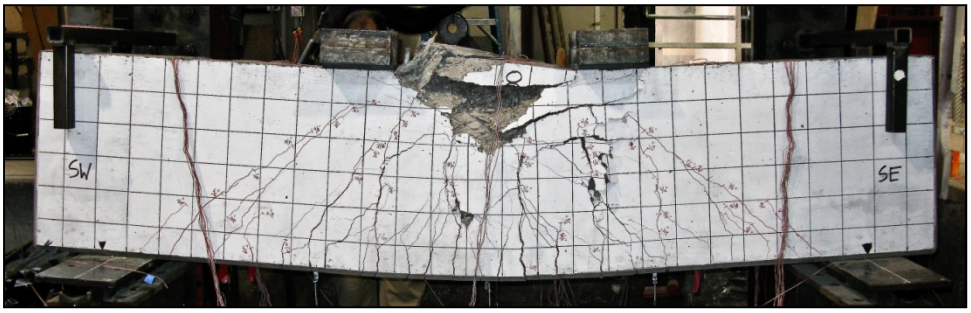

Fig. 4.9 – Failed specimen RST8 (repaired)

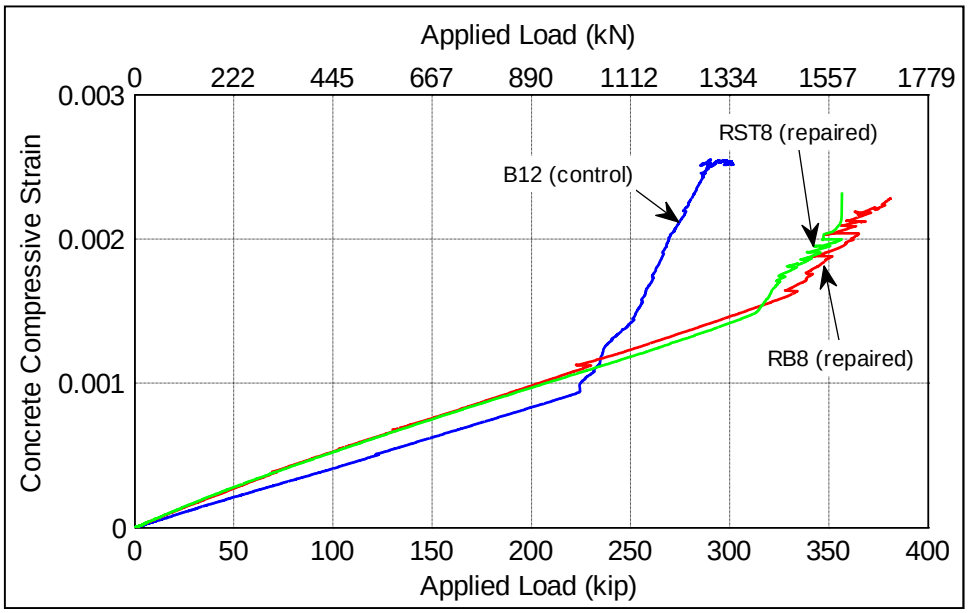

Fig. 4.10 – Concrete compressive strain at midspan vs. applied load (to failure)

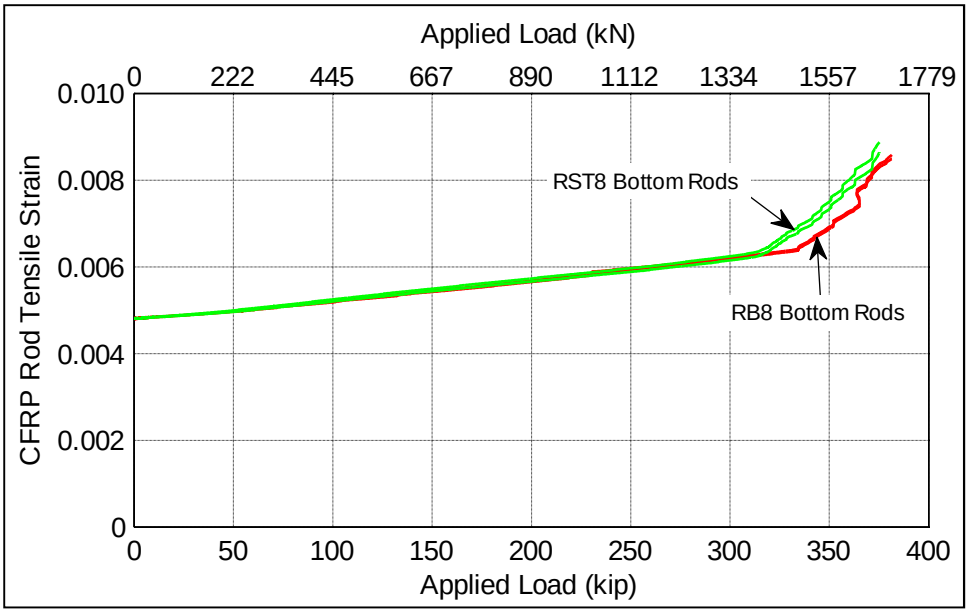

Fig. 4.11 – CFRP Bottom rod strain at midspan vs. applied load to failure

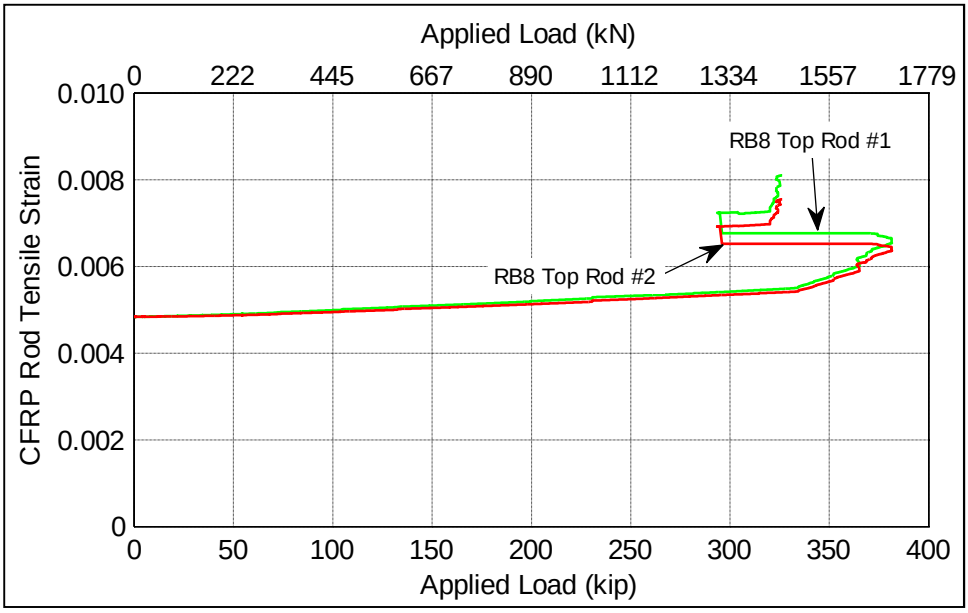

Fig. 4.12 – RB8 CFRP top rod strain at midspan vs. applied load to failure

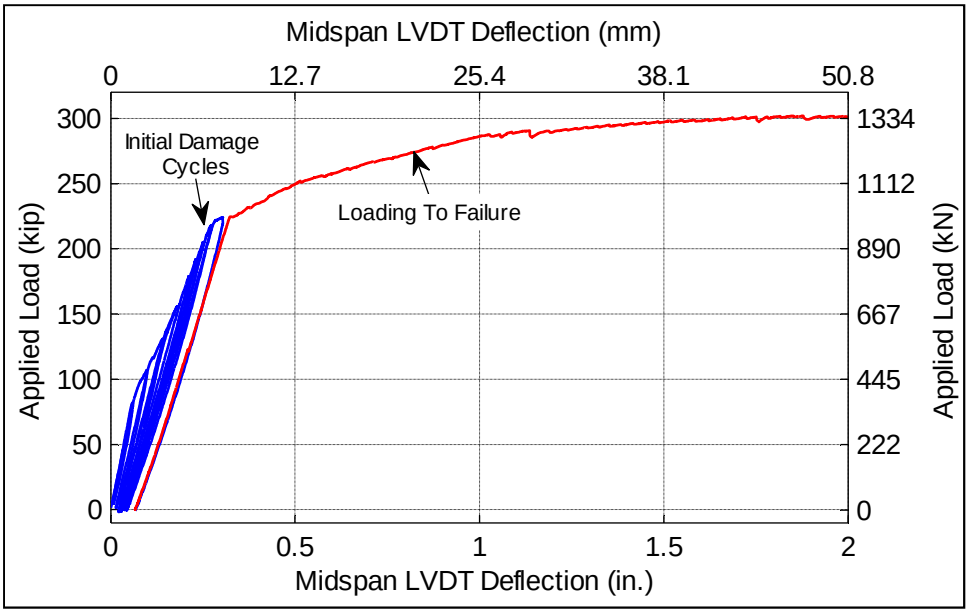

Fig. 4.13 – Applied load vs. midspan deflection for specimen B12 (control)

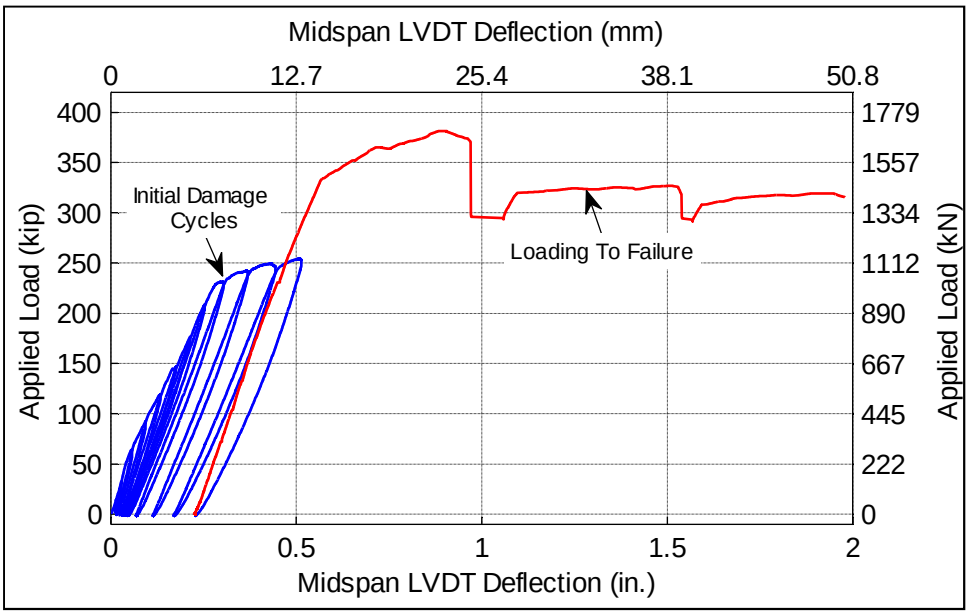

Fig. 4.14 – Applied load vs. midspan deflection for specimen RB8 (repaired)

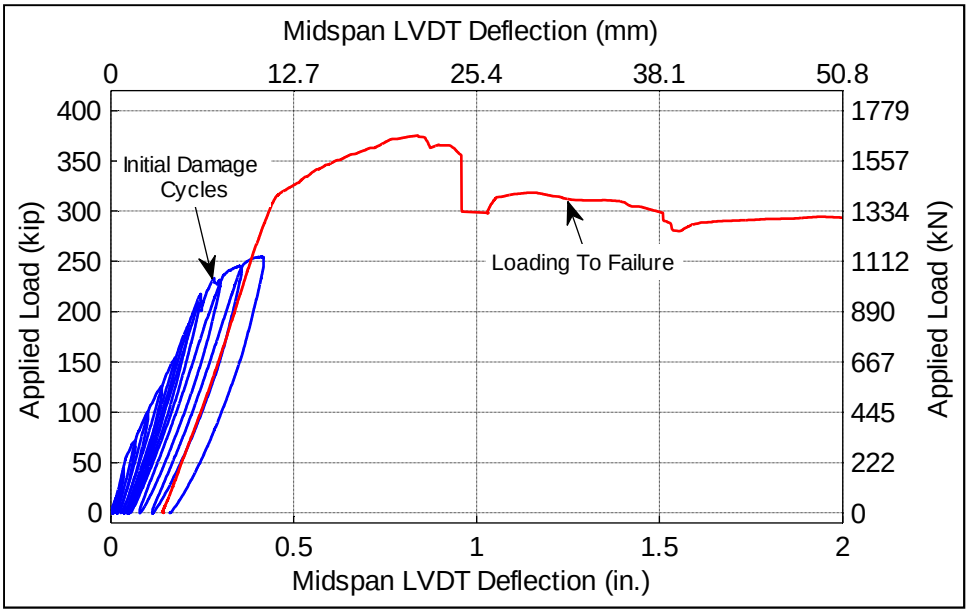

Fig. 4.15 – Applied load vs. midspan deflection for specimen RST8 (repaired)

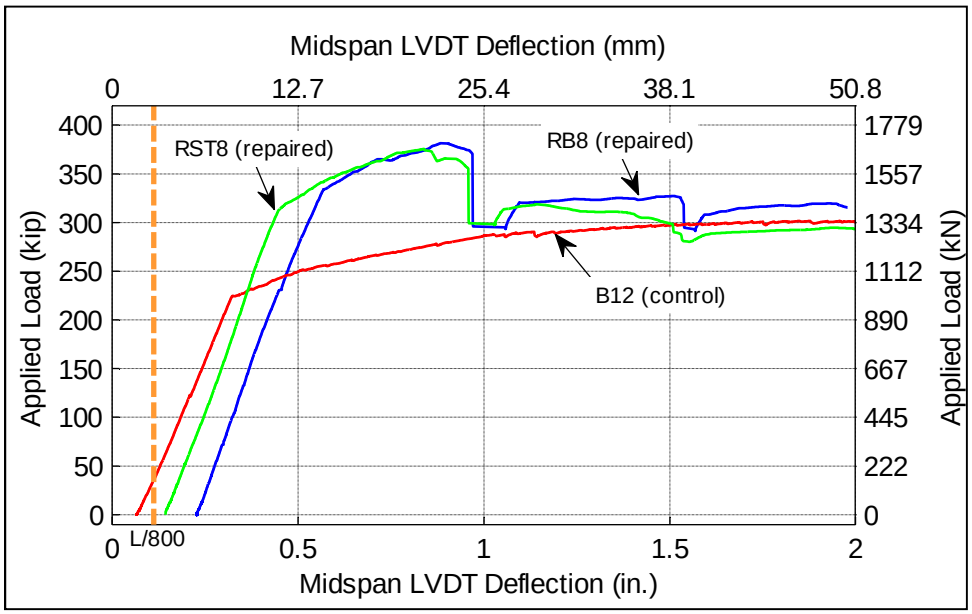

Fig. 4.16 – Applied load vs. midspan deflection for RC specimens loaded to failure

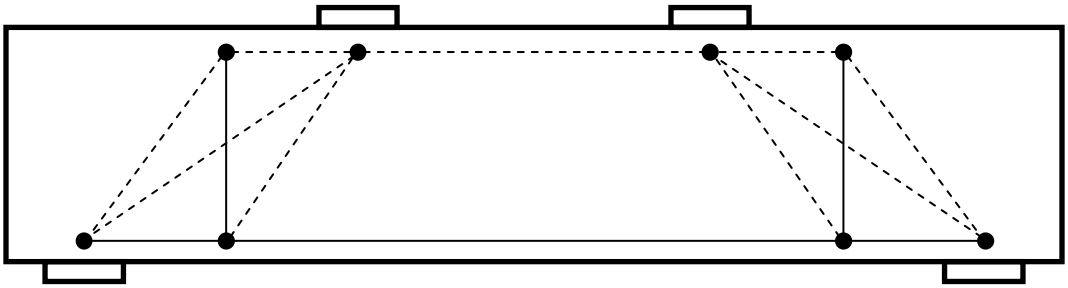

Fig. 4.17 – Strut-and-tie model for specimen B12 (control)

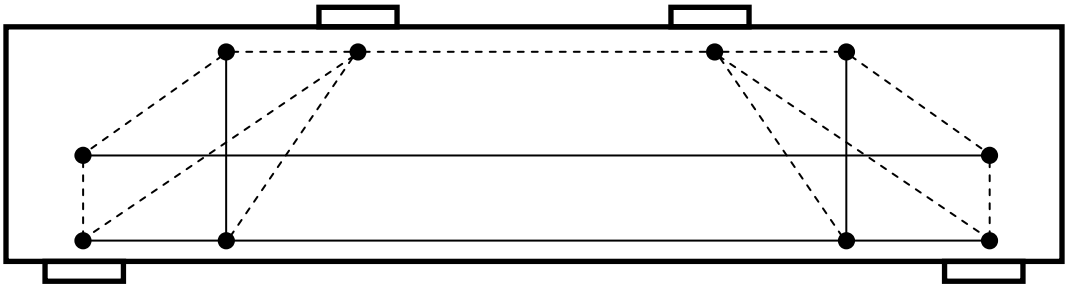

Fig. 4.18 – Strut-and-tie model for specimens RB8 (repaired) and RST8 (repaired)

CHAPTER 5

FLEXURAL REPAIR OF PRESTRESSED CONCRETE BEAMS WITH DAMAGED STEEL TENDONS USING POST-TENSIONED CFRP RODS

Clayton A. Burningham, Chris P. Pantelides, and Lawrence D. Reaveley

Clayton A. Burningham is a PhD candidate in the department of Civil and Environmental Engineering at the University of Utah. He received his bachelor's and MS degrees from the University of Utah.

ACI member **Chris P. Pantelides** is a Professor and Associate Chair of Civil and Environmental Engineering at the University of Utah. He received his bachelor's degree from the American University of Beirut and his MS and PhD from the University of Missouri-Rolla. His research interests include the seismic design, evaluation, and rehabilitation of reinforced concrete buildings and bridges.

Lawrence D. Reaveley is a Professor and former Department Chair of Civil and Environmental Engineering at the University of Utah. He received his bachelor's and MS degrees from the University of Utah and his PhD from the University of New Mexico. His research interests include structural dynamics with an emphasis on earthquake engineering, vibration problems, and seismic rehabilitation.

(To be submitted for publication)

5.1 Abstract

This paper presents research implementing unibody clamp anchors and a simple mechanical stressing device to post-tension external, unbonded carbon FRP (CFRP) rods. The repair system was applied to two scaled prestressed concrete beams representing damaged bridge girders. Damage consisted of cracked concrete and severed internal steel tendons from simulated vehicle collision and/or corrosion. The CFRP repair system performed well, increasing the ultimate strength and flexural capacity of the damaged beams to meet or exceed the capacity of the control specimen. Additionally, an analytical model considering the tendon stress at ultimate and the distribution of internal forces was developed to explore design recommendations for the use of the unibody clamp anchors and stressing device.

Keywords: CFRP, post-tensioning, prestressed concrete, flexural repair, retrofit, beams

5.2 Introduction

Many bridges in the Unites States have reached the end of their design life and show signs of ageing and damage such as corrosion of steel reinforcement, large cracks, and missing concrete cover. Damage to concrete cover and internal steel prestressing tendons can occur when large vehicles attempt to pass under a bridge without adequate clearance. Vehicular impact can fracture the concrete, expose the internal steel prestressing tendons, and/or sever all or part of the outer steel prestressing tendons. Even if the tendons are not severed, removal of the protective concrete cover accelerates the corrosion process. Additionally, cracking from overloading or fatigue could facilitate corrosion of internal steel prestressing tendons. Damage to internal steel prestressing

tendons decreases flexural capacity, and bridges exhibiting these symptoms could be in critical need of replacement, repair, or strengthening.

Typically, girder replacement is expensive, time consuming, and intrusive; therefore, repair or retrofit is often the preferred option. One system used for repair applications is external post-tensioning. This repair method not only restores flexural capacity, but can also mitigate the effects of an increase in service load and help with serviceability considerations such as deflection; thus, external post-tensioning is an excellent option for repairing concrete bridge girders with damage to internal steel prestressing tendons. Traditionally, external post-tensioning has been implemented with high-strength steel tendons because of low material cost, material availability, and ease of installation. However, despite its historic use, steel is susceptible to corrosion, limiting its useful lifespan and requiring extensive protection from deicing salt and moisture.

The limitations of steel tendons can be overcome in external post-tensioning applications by the use of fiber reinforced polymer (FRP) materials. FRP materials are advantageous because of their corrosion resistance and high specific strength. Additionally, the use of FRP materials is becoming increasingly attractive as the price of FRP composites decreases. Several studies have shown that post-tensioned FRP tendons can contribute to flexural strength in new construction (Abdel Aziz et al. 2005; El-Hacha and Elbadry 2006; Täljsten and Nordin 2007); however, few studies have shown the usefulness of post-tensioned FRP tendons in flexural repair and retrofit applications (Elrefai et al. 2007). As a result, additional research is required to investigate the suitability of post-tensioned FRP tendons for the repair of severe flexural damage.

Widespread use of FRP tendons in post-tensioning applications has been slow because of the difficulty in developing a suitable tendon anchor. However, research conducted at the University of Utah has produced a unibody clamp anchor and mechanical stressing device for use in post-tensioning carbon fiber reinforced polymer (CFRP) rods. The clamp anchors are machined from a single piece of steel, and the clamping force is provided by high strength bolts. Further research is needed to analyze the effectiveness of the complete post-tensioning system consisting of the CFRP rods, unibody clamp anchors, and mechanical stressing device when applied to prestressed concrete members.

The research in this paper is concerned with applying CFRP rods, unibody clamp anchors, and the above-mentioned mechanical stressing device as a complete FRP strengthening system for the flexural repair of damaged prestressed concrete beams. The specific damage considered during this research was damage resulting from impact with vehicles passing underneath a bridge without adequate clearance. Such impact could result in severed internal steel prestressing tendons or removal of concrete cover and subsequent corrosion of internal steel prestressing tendons. An illustrative example of impact damage observed on an actual prestressed concrete bridge girder can be seen in Fig. 5.1.

The paper includes details of testing methods, specimen design and fabrication, experimental design, and an analysis of results. Additionally, the methods used for collecting data during laboratory testing as well as details pertaining to the performance and effectiveness of the FRP repair system and its application are provided—with specific focus on the performance of the CFRP tendons and their ability to repair

damaged beams. Finally, an analytical model considering the tendon stress at ultimate and conventional beam theory is presented to explore design recommendations for the use of the unibody clamp anchors and mechanical stressing device.

5.3 Research Significance

Previous research on using external post-tensioned CFRP tendons for repair of damaged concrete beams has been limited. This research presents the implementation of unibody clamp anchors and a simple mechanical stressing device for the repair of prestressed concrete beams with post-tensioned CFRP rods. In addition, the paper validates equations from the literature for evaluating the ultimate stress of unbonded post-tensioned CFRP rods. Furthermore, the CFRP repair system implemented in this research could facilitate the acceptance of CFRP post-tensioning systems in the construction industry.

5.4 Experimental Investigation

5.4.1 Specimen Fabrication

Three scaled prestressed concrete (PC) beam specimens were designed and fabricated for testing. The three beams (specimens P2, RP1, and RP3 with “R” indicating a specimen to which the repair system was applied) were manufactured by a local PCI-certified precast/prestressed concrete company. The precast girders measured 12” (305 mm) wide x 20” (508 mm) tall x 15’ (4.57 m) long, and each prestressed beam had three ½ inch (13 mm) 7-wire low-relaxation prestressing steel strands with an ultimate strength of 270 ksi (1862 MPa). Additionally, the prestressed beams had #3 (ø 10 mm) stirrups placed at 12” (305 mm) on center. The location of internal reinforcement can be seen in Fig. 5.2, and Table 5.1 provides a summary of specimen reinforcement and geometry.

5.4.2 Experimental Design

All of the beams were tested in the University of Utah Structural Testing Laboratory. To achieve the simulation of field observed vehicle impact damage, the beams were subjected to initial damage using a four point loading system. A hydraulic actuator with a 500 kip (2220 kN) inline load cell and a steel spreader beam were used to apply a two point load, spaced 30” (762 mm) apart, to the top of the specimens, as seen in Fig. 5.3. The specimens were tested with an unbraced length of 13’-8” (4.17 m) and had a depth of 20” (508 mm), producing a shear span to depth ratio (a/d ratio) of 3.35.

5.4.3 Material Properties

The materials used in this research are typical of United States construction. All steel reinforcing bars used in the fabrication of the specimens had a nominal tensile strength of 60 ksi (414 MPa). The CFRP rods used in this research had the following properties as provided by the manufacturer: rod diameter = 3/8 inch (9.53 mm), tensile strength = 27.5 kip (122.3 kN), tensile modulus = 22,500 ksi (155 GPa), and elongation at break = 1.1%. Additionally, the internal steel prestressing tendons were low relaxation ½ in. (13 mm) diameter 7-wire strands with a nominal ultimate strength of 270 ksi (1862 MPa). Concrete cylinder tests performed at 7 days after casting of the steam cured prestressed concrete beams produced a compressive concrete strength of 7.0 ksi (48 MPa), and at the time of specimen testing, the concrete had a compressive strength of 10.0 ksi (69 MPa).

5.4.4 Testing Methods

Load testing was carried out in three phases: damage, repair, and failure. First, damage loading was used to introduce flexural cracking which could lead to accelerated

corrosion of internal steel prestressing tendons. Additionally, specimens RP1 and RP3 underwent further damage with respect to the internal prestressing steel—to simulate more severe impact damage. Subsequently, specimens RP1 and RP3 were repaired with external post-tensioned CFRP rods. Finally, all three specimens were loaded to failure.

5.4.5 Damage Loading

Damage loading applied to specimens P2 and RP1 consisted of half-cycles in compression to induce flexural cracking observed in actual prestressed concrete girders. The loading was displacement controlled to avoid catastrophic failure and subsequent loss of the specimens. Displacement half-cycles were applied in increments of 0.0625 in. (1.59 mm), with the amplitude of each successive half-cycle increasing by 0.0625 in. (1.59 mm). In addition, the rate of displacement was held constant at 0.0625 in./min (1.59 mm/min) throughout the test. All specimens were subjected to the same loading protocol, with termination of loading dependent upon the level of visible cracking, deflected shape data, and applied load versus actuator displacement data. Testing procedures were paused after each half-cycle to aid in crack inspection, marking, and documentation.

Additionally, extensive damage was inflicted upon specimens RP1 and RP3 to simulate damage to internal steel prestressing tendons from vehicle collision and/or subsequent corrosion. Concrete cover was removed from both specimen RP1 and RP3 to expose an outer 7-wire steel prestressing strand within the constant moment region. Next, for specimen RP1, three of the seven wires in this strand were cut—leaving two intact 7-wire strands and one 4-wire strand. For the damage imposed on specimen RP3, no initial cracking loads were applied, but all seven wires of an outer steel prestressing strand were cut, leaving two intact 7-wire strands. These cuts, seen in Fig. 5.4, simulated partial or

complete severing of the exterior tendon on impact in an exterior girder or corrosion of an exterior tendon due to loss of concrete cover and subsequent exposure to the elements.

5.4.6 FRP Repair

After simulating damage to internal steel prestressing tendons in specimens RP1 and RP3, the beams were repaired with external post-tensioned CFRP rods. The unibody clamp anchors and mechanical stressing device seen in Fig. 5.5 were used to introduce the post-tensioning force. Specimens RP1 and RP3 were repaired with two rods, one on each side of the beam along the beam length at a depth of 15” (381 mm) from the top compression fiber. The CFRP rods were post-tensioned to a strain of approximately 0.485%, producing a post-tensioning force of 12 kips (53.4 kN) in each rod. The novel mechanical stressing device implemented in this research consists of a slotted square HSS section running perpendicular to the beam length at both ends of the beam. The slots in the HSS section allow the tendons to pass through the slots such that the unibody clamp anchors make contact with the back side of the tube. On the stressing end of the beam, two sleeve nuts are positioned on top and two on the bottom of the HSS section. The sleeve nuts run parallel with the beam, and tendon stressing occurs when 1.0 in. (25 mm) diameter bolts are screwed into the sleeve nuts; the bolts react against the beam end, moving the HSS section back to stress the tendons. Tightening the stressing bolts in an alternating star pattern ensures the tendons are stressed with controlled increments of tightening.

5.4.7 Loading To Failure

After repairing specimens RP1 and RP3 with external post-tensioned CFRP rods, the specimens were loaded to failure with specimen P2 as the control specimen. The

displacement controlled loading to failure was monotonic at a rate of 0.0625 in./min. (1.59 mm/min.). Termination of the loading depended on failure of the specimen as measured by a 20% decrease from the maximum load or failure of the external post-tensioning, whichever occurred first.

5.5 Experimental Results

5.5.1 Data Collection Methods

All instrumentation data were collected by an electronic data acquisition system at a sampling rate of two data points per second. Instrumentation consisted of strain gauges and linear variable differential transformers (LVDTs). All strain gauge readings were measured in units of microstrain, and all LVDT readings were measured within 0.001 in. (0.025 mm).

5.5.2 Instrumentation

The specimens were instrumented with three LVDTs—one 54.5” (1.38 m) from either end and one at midspan—attached to the bottom of the beam during testing in order to measure the deflected shape under loading. Concrete strain gauges placed at 69.5” (1.77 m) from each end and at midspan on the top of the beams measured the compressive strain in the concrete during testing. Additionally, strain gauges were placed on the CFRP rods at midspan to measure the strain in the tendons for specimens RP1 and RP3.

5.5.3 Specimen Data Analysis

No anchor slippage was observed in any of the CFRP rods during testing of the specimens to failure. Furthermore, the lack of slip demonstrates that the anchors work as designed when applied as a system to post-tension concrete beams.

During testing, specimen P2 (control) failed from concrete compressive failure between the loading points on the top of the beam. Specimen RP1 (repaired) failed from rupture of the external CFRP rods, and specimen RP3 (repaired) failed due to concrete compressive failure between the loading points. Photos of specimen P2 (control) after concrete compressive failure, specimen RP1 (repaired) after rupture of the CFRP rods, and specimen RP3 (repaired) after removal of the unbroken CFRP rods can be seen in Figs. 5.6-5.8, respectively.

For all three specimens, the highest compressive concrete strain was observed at midspan, as seen in Fig. 5.9, which shows the change in concrete compressive strain at midspan with the change in applied load when the specimens were loaded to failure. It can be seen from Fig. 5.9 that specimens P2 and RP3 experienced maximum concrete strains greater than 0.003, indicating that the concrete failed due to crushing. These numerical data correlate well with the failure mode visually observed in specimens P2 and RP3 and seen in Figs. 5.6 and 5.8, respectively.

An increase in the strain in the CFRP rods in specimen RP1 and RP3 was observed during testing of the specimens to failure. The initial strain in the rods from the post-tensioning application was 0.485%. At failure of the external CFRP tendons, the average maximum strain in the CFRP rods was approximately 0.750% and 0.814% for specimen RP1 and RP3, respectively. Since the ultimate strain of the rods is 1.1%, the

most likely explanation for rupture of the rods at lower strains is stress concentrations at a point other than where the strain gauges were located at midspan. One location of possible stress concentrations is near the beam ends due to the rotation of the beam ends at large deflections. The beam end rotation can introduce flexure into the rods rather than pure tension, resulting in stress concentrations. The change in CFRP rod strain at midspan with the change in applied load when specimens RP1 and RP3 were loaded to failure can be seen in Fig. 5.10.

The CFRP repair system was successful—both specimen RP1 and RP3 exhibited an increase in ultimate capacity due to the application of the CFRP repair system. The ultimate load for specimens P2 (control), RP1 (repaired), and RP3 (repaired) was 104 kip (463 kN), 112 kip (498 kN), and 102 kip (454 kN), respectively. For specimen RP1, the ultimate load corresponds to an increase of approximately 7.7% in ultimate capacity from the use of external post-tensioned CFRP rods. However, it should be remembered that specimen RP1 (repaired) had two intact 7-wire strands and one 4-wire strand (three wires were cut), whereas specimen P2 (control) had three intact 7-wire strands. Therefore, application of the theoretical capacity of specimen RP1 (repaired) based on the cut wires produces an effective increase in ultimate capacity of 20.2% from the use of external post-tensioned CFRP rods. Also, although a third of the prestressing force was removed from specimen RP3, the repair with the external post-tensioned CFRP rods produced load-deflection behavior virtually identical to that of the control specimen. This identical behavior implies an effective increase in ultimate capacity of 29.7% from the use of external post-tensioned CFRP rods. The similarities in the performance of specimens P2 (control) and RP3 (repaired) can be seen in Fig. 5.11.

From Fig. 5.11, it can be seen that failure of the CFRP rods for specimen RP1 occurred at a deflection about eight times greater than L/800 (0.21 in. or 5.21 mm), the maximum allowable design deflection under service live loads for concrete bridge construction (AASHTO 2009). Therefore, although failure of the post-tensioned CFRP rods was brittle, failure occurred at a deflection much greater than possible service load deflections. It can also be seen that after failure of the CFRP rods, specimen RP1 (repaired) exhibited a residual strength of approximately 97 kip (431 kN). This residual strength is evidence that complete catastrophic failure of the beam did not occur due to the ductility of the original system. Additionally, it can be concluded from Fig. 5.11 that the residual strength in specimen RP1 (repaired) after failure of the CFRP rods suggests that at large deflections specimen RP1 (repaired) would fail similarly to specimen P2 (control)—from concrete compressive failure between the loading points on the top of the beam.

5.6 Analytical Investigation

Conventional beam theory can be used to predict the ultimate load of the specimens tested in this research. The theoretical capacity of control specimen P2 was calculated to be 73 kip (330 kN). Compared to the actual ultimate load of 104 kip (463 kN), the ratio of the actual to the theoretical ultimate load is 1.42, indicating that the theoretical prediction is in good agreement with the actual value and the design is conservative. To determine the theoretical capacity of specimens RP1 and RP3, the stress in the CFRP rods at ultimate must first be determined. Previous research for post-tensioned steel tendons has shown that strain compatibility can be used to analyze the external tendons as if they were bonded and then apply a strain reduction factor to

account for the tendons actually being unbonded (Naaman et al. 1991). This method of using a strain reduction factor was subsequently suggested that it could be applied to FRP tendons as well (Naaman et al. 2002; ACI Committee 440 2004). Therefore, Eq. (5.1) can be used to determine the stress at ultimate in the external, unbonded post-tensioned CFRP rods used in this research

$$f_{p\_CFRP} = f_{pe\_CFRP} + \Omega_u E_{CFRP} \varepsilon_{cu} \left(\frac{d_{CFRP}}{c_u} - 1 \right) \quad (5.1)$$

where c_u is the depth to the neutral axis at ultimate; d_{CFRP} is the depth to the CFRP rods, 15” (381 mm); E_{CFRP} is the modulus of elasticity of the CFRP rods, 22,500 ksi (155 GPa); f_{p_CFRP} is the stress in the CFRP rods at ultimate; f_{pe_CFRP} is the effective prestress in the CFRP rods, 109 ksi (752 MPa); Ω_u is the strain reduction factor; and ε_{cu} is the failure strain of concrete in compression, 0.003.

Suggested values for the strain reduction factor depend on the type of loading. The research presented in this paper is best described as center point loading since the distance between loading points on the top of the beams was only 30” (762 mm) compared to an unbraced length of 13’-8” (4.17 m). Hence, for the specimens in the current research Eq. (5.2), which has been standardized such that the predicted value is likely to be smaller than the experimental result, was used to calculate the strain reduction factor

$$\Omega_u = \frac{1.5}{L/d_{CFRP}} \quad (5.2)$$

where L is the unbraced length of the beam, 13'-8" (4.17 m). The use of Eq. (5.2) results in a strain reduction factor of 0.137. Additionally, appropriate values of c_u can be calculated from the following equation

$$c_u = \frac{-B+\sqrt{B^2-4AC}}{2A} \tag{5.3}$$

where

$A = 0.85f'_c b\beta_1$;

$B = A_{CFRP}\left(E_{CFRP}\varepsilon_{cu}\Omega_u - f_{pe\_CFRP}\right) - A_s f_y - A_{ps}f_{ps}$; and

$C = -A_{CFRP}E_{CFRP}\varepsilon_{cu}\Omega_u d_{CFRP}$

In the above expressions, A_{CFRP} is the area the of post-tensioned CFRP rods, 0.22 in^2 (142 mm^2); A_{ps} is the area of internal steel prestressing strands; A_s is the area of tensile mild steel reinforcement, 0.62 in^2 (400 mm^2); b is the beam width, 12" (305 mm); f'_c is the compressive strength of the concrete, 10.0 ksi (69 MPa); f_{ps} is the prestressing force in the internal steel strands, 243 ksi (1.68 GPa); f_y is the yield stress of the mild steel reinforcement, 60 ksi (414 MPa); and β_1 is 0.65. The use of Eq. (5.3) produces c_u values of 2.00" (50.9 mm) and 1.72" (43.7 mm) for specimens RP1 and RP3, respectively. The resulting CFRP rod ultimate stresses predicted by Eq. (5.1) are 169 ksi (1167 MPa) for specimen RP1 and 181 ksi (1245 MPa) for specimen RP3. These values of theoretical ultimate CFRP rod stress compared to values of measured ultimate CFRP rod stress (from strain gauges on the rods) result in errors of 0.27% and 1.4% for specimens RP1 and RP3, respectively. Thus, Eq. (5.1) has excellent prediction capability.

Furthermore, conventional beam theory leads to the following equation for ultimate moment capacity

$$M_u = A_{ps} f_{ps} \left(d_{ps} - \frac{a}{2}\right) + A_s f_y \left(d - \frac{a}{2}\right) + A_{CFRP} f_{p\_CFRP} \left(d_{CFRP} - \frac{a}{2}\right) \quad (5.4)$$

where M_u is the ultimate moment capacity; a is the depth of the equivalent compression block equal to $\beta_1 c_u$; and d is the depth to the mild steel reinforcement, 15" (381 mm). Next, from the ultimate moment capacity, the ultimate load, P_u, can be found from the following equation

$$P_u = \frac{2M_u}{0.5(L-s)} \quad (5.5)$$

where s is the spacing between load points on the top of the beam, 30" (762 mm), as shown in Fig. 5.3.

Key values used in calculating the theoretical ultimate load from Eq. (5.5) can be seen in Table 5.2, and the use of Eq. (5.5) results in theoretical ultimate capacities of 83 kip (371 kN) for RP1 and 73 kip (330 kN) for RP3. Consequently, the corresponding ratios of actual to theoretical ultimate load are 1.36 and 1.39 for specimens RP1 and RP3, respectively. Similar to the ratio of 1.42 found for control specimen P2, these ratios show that the theoretical ultimate loads are in good agreement with the actual measured ultimate loads, and that the design is conservative. A summary of the experimental and theoretical ultimate loads are given in Table 4.2. Furthermore, the ratios of actual to theoretical ultimate load and the percent error between the actual and theoretical stress in the CFRP rods at ultimate indicate that Eq. (5.1) and Eq. (5.2) are appropriate for predicting the stress in the CFRP rods at ultimate when calculating the theoretical

ultimate capacity of prestressed concrete members repaired with the system of unibody clamp anchors, mechanical stressing device, and CFRP rods used in the current research.

5.7 Conclusions

Based upon the experiments carried out in this research, it can be concluded that specimens RP1 and RP3 were successfully repaired using an external post-tensioning system consisting of CFRP rods, unibody clamp anchors, and a mechanical stressing device. Repaired specimens RP1 and RP3 showed an effective increase in ultimate strength of 20.2% and 29.7%, respectively. This increase in ultimate strength of specimen RP1 (repaired) compared to specimen P2 (control) and the similar performance of specimen P2 (control) and RP3 (repaired) demonstrate that external post-tensioned CFRP rods are able to compensate for partial or complete removal of a prestressing tendon.

Moreover, it was found that although the repaired specimen RP1 failed as a result of rupture of the external post-tensioned CFRP rods, the rupture occurred at deflections much greater than those expected from service loads. Additionally, residual capacity was present after CFRP rod rupture. This is significant in that catastrophic beam failure did not occur even though the CFRP rods failed in tension.

It was found that theoretical expressions from the literature may be used to predict the stress at ultimate in the CFRP tendons used in this research as well as the ultimate capacity of the beams. As demonstrated by this successful research, post-tensioning CFRP rods using unibody clamp anchors and a mechanical stressing device is feasible for the repair of concrete beams with severe damage to internal steel prestressing tendons; it is recommended that further studies be carried out to assess the possibility for field application of the system and to assess the suitability of the repair system for general use.

It is also recommended that further studies be carried out to determine the suitability of the anchors for use as a coupling device with the CFRP rods. The successful implementation of the anchors and CFRP rods in this research strongly suggests that the anchors could potentially be used to join two sections of CFRP rod, facilitating post-tensioning of longer spans that are typical of actual bridges.

Although the repair system investigated in this paper was successful, it requires access to the end of beams which is not always available in field applications. However, for use of the CFRP repair system implemented in this research, only 18” (0.46 m) of free space is required behind the beams. In the challenging situation where absolutely no end access is available, or the length of end access is less than the minimum, the system could be attached to the bottom surface or web area near the beam ends with mechanical anchorage. This solution would allow the system studied in this research to post-tension essentially the entire length of the beam without requiring any beam end access.

5.8 Acknowledgements

The authors wish to acknowledge the financial support of the Utah Department of Transportation and the University of Utah. The authors would also like to acknowledge the contributions of Hanson Structural Precast and Sika Inc. Additionally, the authors would like to thank Brandon Besser, Mark Bryant, Megan Crump, Jack Furbush, Mike Gibbons, Ruifen Liu, Yasuteru Okahashi, Brett Raddon, Eric Smith, Max Wood, and Arthur Yeomans for their assistance in specimen fabrication and testing.

5.9 Notation

A_{CFRP} = area of post-tensioned CFRP rods

A_{ps} = area of internal steel prestressing strands

A_s = area of tensile mild steel reinforcement

a = depth of equivalent compression block

c_u = depth to neutral axis at ultimate

d = depth of mild steel reinforcement

d_{CFRP} = depth to CFRP rods

E_{CFRP} = modulus of elasticity of CFRP rods

f'_c = compressive strength of concrete

f_{p_CFRP} = stress in CFRP rods at ultimate

f_{pe_CFRP} = effective prestress in CFRP rods

f_{ps} = prestressing force in internal steel strands

f_y = yield stress of mild steel reinforcement

L = unbraced length of beam

M_u = ultimate moment capacity

s = spacing between load points on top of the beam

β_1 = factor relating depth of equivalent compression block to depth of neutral axis

ε_{cu} = failure strain of concrete in compression

Ω_u = strain reduction factor

5.10 References

Abdel Aziz, M.; Abdel-Sayed, G.; Ghrib, F.; Grace, N.; and Madugula, M., 2005, "Analysis of Concrete Beams Prestressed and Post-Tensioned with Externally Unbonded Carbon Fiber Reinforced Polymer Tendons," *Canadian Journal of Civil Engineering*, V. 31, pp. 1138-1151.

ACI Committee 440, 2004, "Prestressing Concrete Structures with FRP Tendons (ACI 440.4R-04)," American Concrete Institute, Farmington Hills, MI.

AASHTO, 2009, “AASHTO LRFD Bridge Design Specifications (4th Edition),” American Association of State Highway and Transportation Officials, Washington DC.

El-Hacha, R., and Elbadry, M., 2006, “Strengthening Concrete Beams With Externally Prestressed Carbon Fiber Composite Cables: Experimental Investigation,” *PTI Journal*, V. 4, No. 2, pp. 53-70.

Elrefai, A.; West, J.; and Soudki, K., 2007, “Strengthening of RC Beams with External Post-Tensioned CFRP Tendons,” ACI SP-245-8, pp. 123-142.

Naaman, A., and Alkhairi, F., 1991, “Stress at Ultimate in Unbonded Post-Tensioning Tendons: Part 2 - Proposed Methodology,” *ACI Structural Journal*, V. 88, No. 6, pp. 683-692.

Naaman, A.; Burns, N.; French, C.; Gamble, W.; and Mattock, A., 2002, “Stresses in Unbonded Prestressing Tendons at Ultimate: Recommendation,” *ACI Structural Journal*, V. 99, No. 4, pp. 518-529.

Täljsten, B., and Nordin, H., 2007, “Concrete Beams Strengthened with External Prestressing Using External Tendons and Near-Surface-Mounted Reinforcement,” ACI SP-245, pp. 143-164.

Table 5.1 – Specimen geometry and reinforcement details

Width	Height	Length	Shear Reinforcement	Flexure Reinforcement
12” (305 mm)	20” (508 mm)	15’ (4.57 m)	#3 (ø 10mm) stirrups at 12” (305 mm)	3 - ½ in. (13 mm) 7 wire tendons

Table 5.2 – Data for calculation of theoretical values at ultimate

Specimen	f_{p_CFRP}	c_u	A_{ps}	a	M_u
RP1 (repaired)	169 ksi (1167 MPa)	2.00” (50.9 mm)	0.393 in^2 (254 mm^2)	1.30” (33.1 mm)	231 kip-ft (313 kN-m)
PR3 (repaired)	181 ksi (1245 MPa)	1.72” (43.7 mm)	0.306 in^2 (197 mm^2)	1.12” (28.4 mm)	205 kip-ft (278 kN-m)

Table 5.3 – Experimental and theoretical ultimate loads

Specimen	Experimental Ultimate Load	Theoretical Ultimate Load	Ratio of Experimental to Theoretical Ultimate Load
P2 (control)	104 kip (463 kN)	73 kip (330 kN)	1.42
RP1 (repaired)	112 kip (498 kN)	83 kip (371 kN)	1.36
PR3 (repaired)	102 kip (454 kN)	73 kip (330 kN)	1.39

Fig. 5.1 – Girder damage from vehicle impact

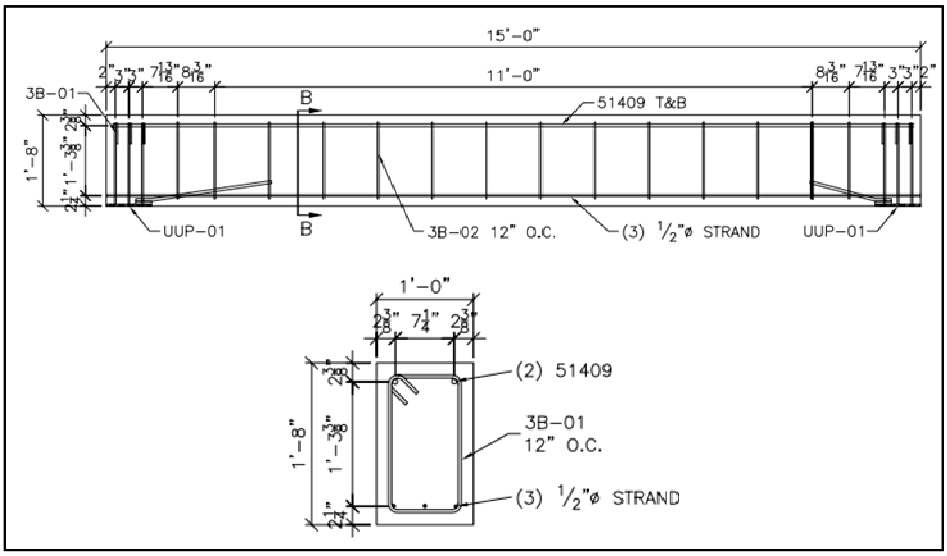

Fig. 5.2 – Reinforcement layout for specimens P2, RP1, and RP3
(1” = 25.4 mm; 1’ = 0.305 m)

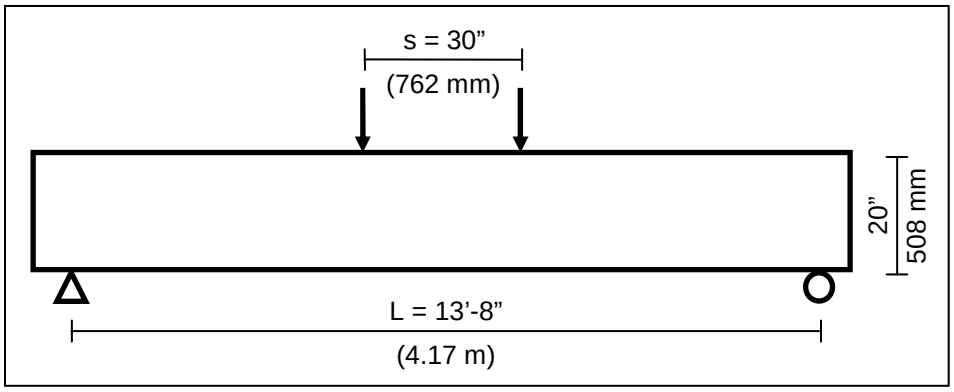

Fig. 5.3 – Test setup

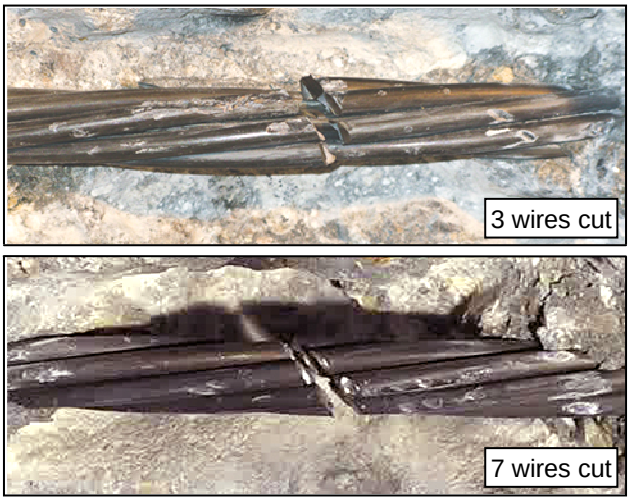

Fig. 5.4 – Damaged outer steel tendon in specimen RP1 (top) and RP3 (bottom)

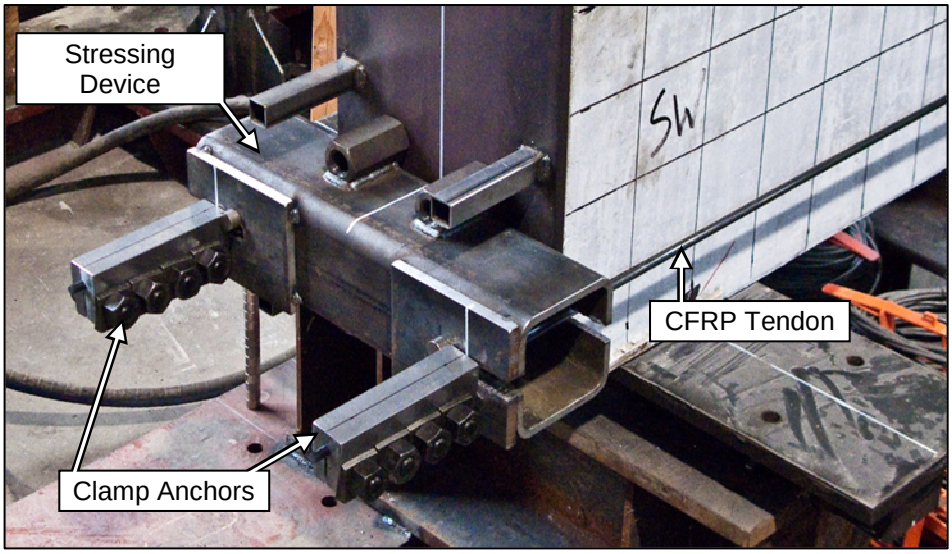

Fig. 5.5 – End view of stressing system

Fig. 5.6 – Failed specimen P2 (control), Grid = 4” (100 mm)

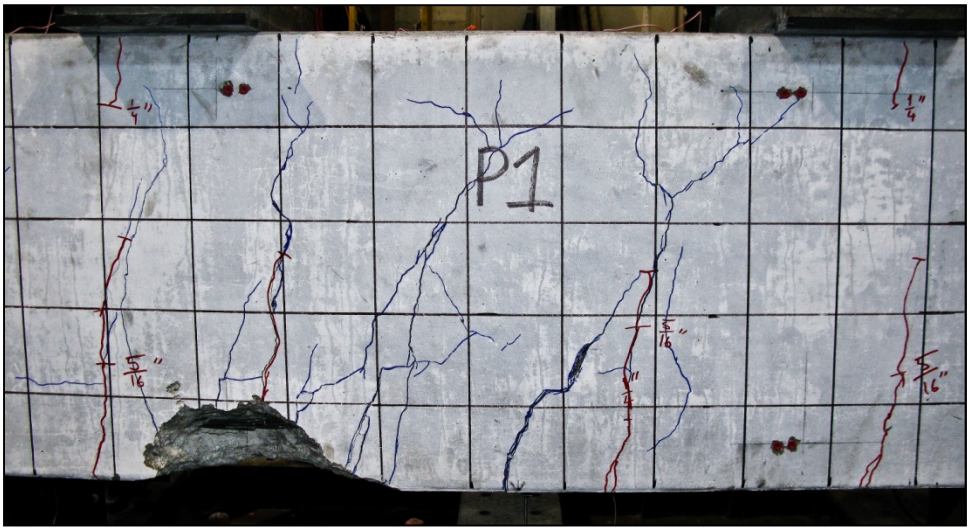

Fig. 5.7 – Failed specimen RP1 (repaired), Grid = 4” (100 mm)

Fig. 5.8 – Failed specimen RP3 (repaired), Grid = 4” (100 mm)

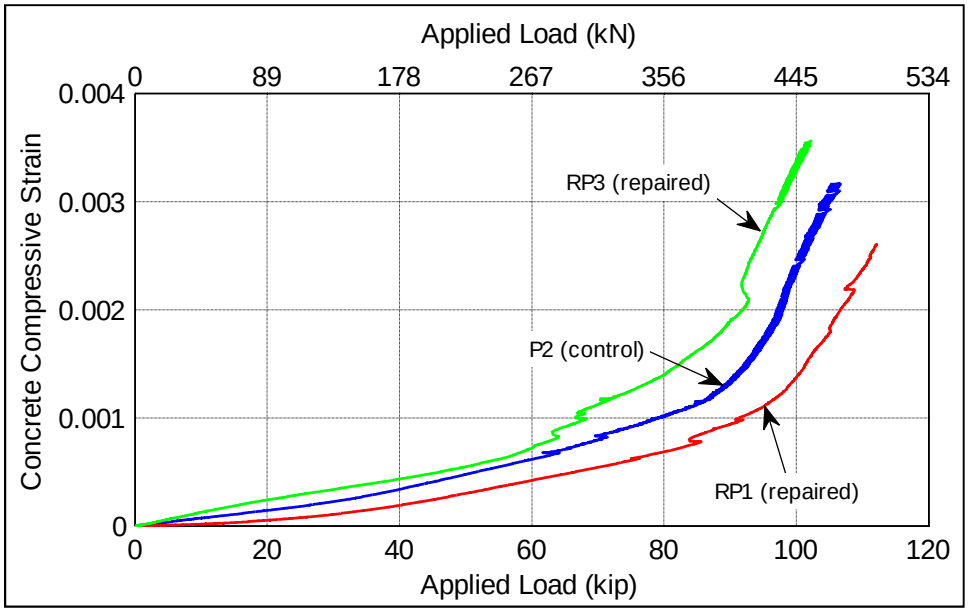

Fig. 5.9 – Concrete compressive strain at midspan vs. applied load (to failure)

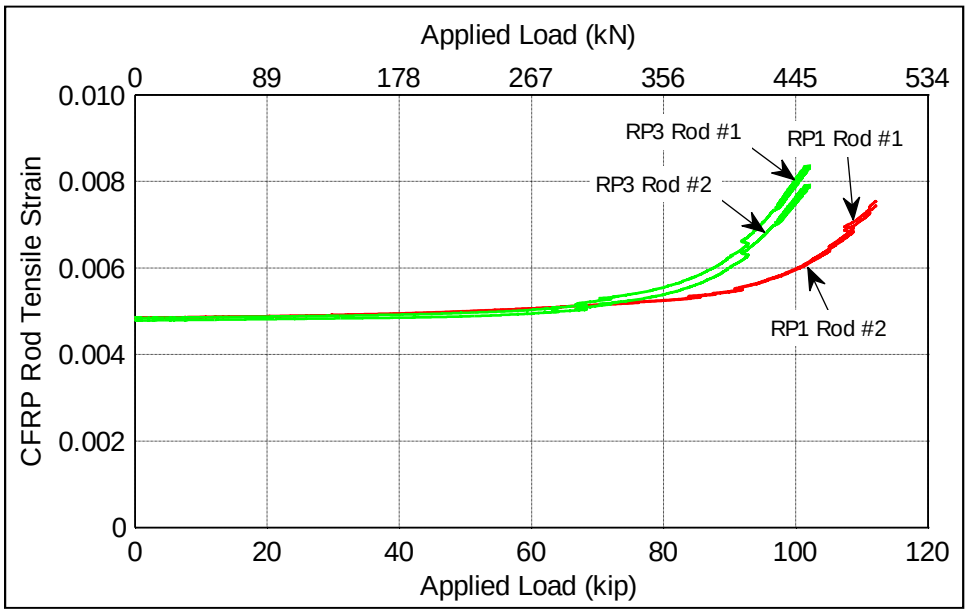

Fig. 5.10 – CFRP rod strain at midspan vs. applied load (to failure)

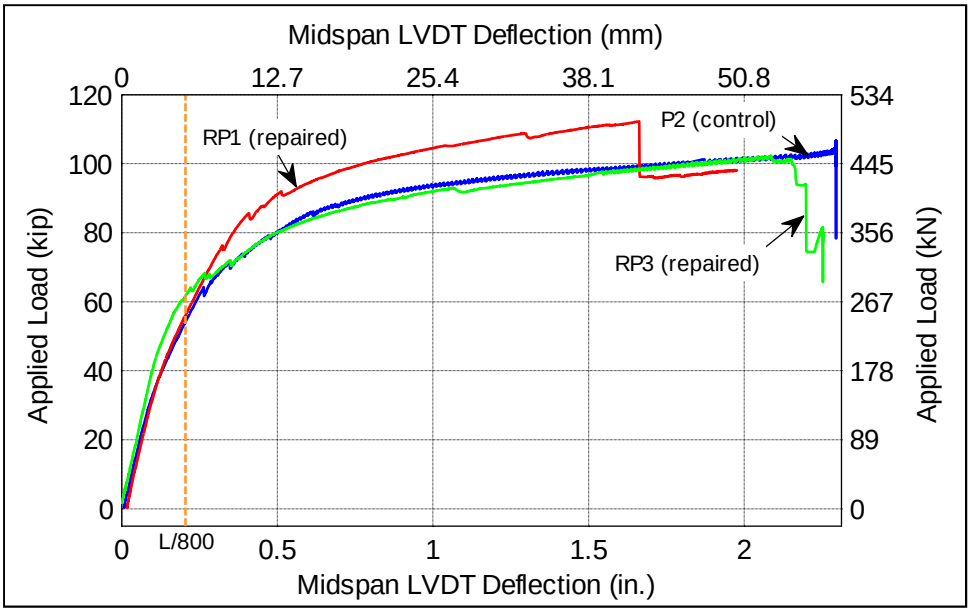

Fig. 5.11 – Applied load vs. midspan deflection for loading to failure

CHAPTER 6

SUMMARY AND CONCLUSIONS

The research presented in this dissertation has resulted in the following accomplishments. First, a unibody clamp anchor was developed to demonstrate that a simple and economical anchor can be used to control slip and achieve effective post-tensioning of CFRP rods. Second, a novel mechanical stressing device was developed to reduce the required space behind a member during the post-tensioning process. Furthermore, the mechanical stressing device functions with a single anchor at the stressing end—as opposed to the current two anchor requirement. Lastly, equations and methods in the literature were assessed to determine their applicability to the specimens considered in this research. An examination of the abovementioned achievements detailed in Chapters 3-5 results in several observations:

1) The unibody clamp anchors developed in this research employ a simple geometry absent of complicated wedges, bevels, and multiple pieces, resulting in an anchor that requires less machining as compared to previously developed anchors discussed in the literature.
2) With an anchor efficiency of 84% (when compared to the rod manufacturer specified ultimate tensile capacity), the generation IV anchor performed the best out of the four generations considered in this research.

3) The inclusion of extra anchor length in the generation IV design controlled stress concentrations, as evidenced by the 37% reduction in contact pressure between the steel anchor and CFRP rod at the lead edge.
4) The tapered outer slot included in the generation IV anchor allowed for an increase in the clamping force as compared to other generations because it prevented the edges of the outer slot from touching.
5) The novel mechanical stressing device allowed the repair system in this paper to be implemented in laboratory testing with a single unibody clamp anchor at the stressing end and a minimum requirement of 18” (0.46 m) of free space behind the beam—a space requirement much less than the prerequisite for current hydraulic jacking procedures.
6) As evidenced by the respective 27% and 25% increase in ultimate strength as compared to control specimen B12, the diagonal shear cracking damage imposed upon specimens RB8 and RST8 was successfully repaired with the unibody clamp anchors, mechanical stressing device, and CFRP rods implemented in this study.
7) Repaired specimens RP1 and RP3 showed an effective increase in ultimate strength of 20.2% and 29.7% as compared to control specimen P2, respectively. This increase in ultimate strength is evidence that external post-tensioned CFRP rods were able to compensate for partial or complete removal of a prestressing tendon.
8) Rupture of the post-tensioned CFRP rods applied to damaged laboratory specimens RB8, RST8, RP1, and RP3 occurred at deflections eight times larger

than the AASHTO maximum allowable deflection, indicating a high level of safety regarding serviceability requirements.

9) Residual capacity was present after CFRP rod rupture for specimens RB8, RST8, RP1, and RP3. This is significant in that catastrophic beam failure did not occur even though the CFRP rods failed in tension.

10) A strut-and-tie model produced higher ratios of experimental to theoretical ultimate load for repaired specimens RB8 and RST8 than control specimen B12, signifying that a strut-and-tie model may be used to design the repair system considered in this research when it is to be applied to structural members with similar characteristics as the shear controlled specimens employed in this research.

11) Equation (4.4) from the literature which was originally developed for use with reinforced concrete beams was found to predict the ultimate capacity of repaired specimens RB8 and RST8 within 6%, but was unconservative. Therefore, it is suggested that further research be conducted to calibrate the equation for use with high strength concrete beams with post-tensioned external CFRP tendons.

12) The theoretical expression from the literature found in Eq. (5.1) may be used to predict the stress at ultimate in the CFRP tendons used in this research as well as the ultimate capacity of repaired specimens RP1 and RP3.

CHAPTER 7

FUTURE CONSIDERATIONS

This research represents a successful study on a limited set of laboratory specimens. Furthermore, the results from the finite element analysis are based on assumptions of simple bilinear stress-strain behavior of the steel anchor. Additional analysis is required to verify the results of the simple model and optimize the design of the unibody clamp anchor. Although an anchor efficiency of 84% was observed with the generation IV anchor, it is recommended that additional studies be conducted to reach a design providing 95% efficiency. This is not to say that anchors providing a lesser efficiency are not useful; however, an increase in efficiency economizes the use of advanced composite materials such as CFRP rods in the construction industry.

To accomplish unibody anchor optimization, it is suggested that variables such as anchor thickness and length be explored. The effects of varying the applied torque to each bolt in the anchor should also be investigated. It is possible that the effect of extra length at the lead end of the anchor may be replicated by simply reducing the torque applied to the lead bolt, resulting in a shorter anchor. This exploration is essential as any reduction in anchor length would be beneficial for repair applications where access space is limited. Future design iterations should ensure that anchor slip does not occur while minimizing anchor length. Additionally, corrosion of the unibody anchor must be considered with an investigation into stainless steel or other corrosion resistant materials.

In addition to optimizing the unibody anchor design, future research should implement the unibody clamp anchors and mechanical stressing device in field applications. This would verify the efficacy of the repair system in the field as well as in the laboratory. Other applications of the unibody clamp anchors appropriate for further study include the use of the anchors as a coupling device for the CFRP rods. The successful implementation of the anchors and CFRP rods in this research suggests that the anchors could potentially be used to join two sections of CFRP rod, facilitating post-tensioning of longer spans typical of actual bridges.

With respect to design methods, additional studies should be conducted to determine the suitability of strut-and-tie models in situations where high strength concrete members are repaired with external post-tensioned CFRP tendons.

Lastly, although the repair system investigated in this paper was successful, it requires access to the end of beams which is not always available in field applications. Although the minimum requirement for free space behind the beams was reduced to only 18” (0.46 m), in some field applications such access may not be available. In the challenging situation where absolutely no end access is available, or the length of end access is less than the minimum, the system could be attached to the bottom surface or web area near the beam ends with mechanical anchorage. This solution would allow the repair system developed in this research to post-tension essentially the entire length of the beam without requiring any beam end access.